

The Demographics of Terrestrial Planets in the Venus Zone

COLBY OSTBERG,¹ STEPHEN R. KANE,¹ ZHEXING LI,¹ EDWARD W. SCHWIETERMAN,¹ MICHELLE L. HILL,¹ KIMBERLY BOTT,¹ PAUL A. DALBA,^{2,*} TARA FETHEROLF,^{1,†} JAMES W. HEAD,³ AND CAYMAN T. UNTERBORN⁴

¹Department of Earth and Planetary Sciences, University of California, Riverside, CA 92521, USA

²Department of Astronomy and Astrophysics, University of California, Santa Cruz, CA 95064, USA

³Department of Earth, Environmental and Planetary Sciences, Brown University, Providence, RI 02912, USA

⁴Southwest Research Institute, San Antonio, TX 78238, USA

ABSTRACT

Understanding the physical characteristics of Venus, including its atmosphere, interior, and its evolutionary pathway with respect to Earth, remains a vital component for terrestrial planet evolution models and the emergence and/or decline of planetary habitability. A statistical strategy for evaluating the evolutionary pathways of terrestrial planets lies in the atmospheric characterization of exoplanets, where the sample size provides sufficient means for determining required runaway greenhouse conditions. Observations of potential exoVenuses can help confirm hypotheses about Venus' past, as well as the occurrence rate of Venus-like planets in other systems. Additionally, the data from future Venus missions, such as DAVINCI, EnVision, and VERITAS, will provide valuable information regarding Venus, and the study of exoVenuses will be complimentary to these missions. To facilitate studies of exoVenus candidates, we provide a catalog of all confirmed terrestrial planets in the Venus Zone, including transiting and non-transiting cases, and quantify their potential for follow-up observations. We examine the demographics of the exoVenus population with relation to stellar and planetary properties, such as the planetary radius gap. We highlight specific high-priority exoVenus targets for follow-up observations including: TOI-2285 b, LTT 1445 A c, TOI-1266 c, LHS 1140 c, and L 98-59 d. We also discuss follow-up observations that may yield further insight into the Venus/Earth divergence in atmospheric properties.

Keywords: planetary systems – techniques: photometric – techniques: radial velocities

1. INTRODUCTION

Exoplanets have been discovered at an extraordinary rate over the past several decades, with thousands of confirmed exoplanets now known (Akeson et al. 2013). This large sample of known planets has motivated studies of exoplanet populations/demographics (Tremaine & Dong 2012; Ford 2014; Winn & Fabrycky 2015) and comparison to the Solar System architecture (Limbach & Turner 2015; Martin & Livio 2015; Horner et al. 2020; Kane et al. 2021). Although initial discoveries were dominated by giant planets (Butler et al. 2006; Udry & Santos 2007), subsequent surveys and improved instrumentation have enabled the detection of terrestrial

planets. Radial velocity (RV) surveys have improved dramatically in understanding noise sources and increasing precision (e.g., Pepe et al. 2014; Fischer et al. 2016; Stefansson et al. 2016; Gupta et al. 2021), and legacy RV data have allowed the detection of long-period planets (e.g., Fischer et al. 2014; Butler et al. 2017; Trifonov et al. 2020; Fulton et al. 2021; Rosenthal et al. 2021). In parallel, space-based transit surveys, such as the Kepler mission (Borucki et al. 2010) and the Transiting Exoplanet Survey Satellite (TESS) (Ricker et al. 2015), have pushed the sensitivity of exoplanet experiments deeply into the terrestrial regime.

A significant challenge in characterizing the terrestrial planet population is the modeling of their potential surface conditions (Way et al. 2017; Fauchez et al. 2021; Wolf et al. 2022). A subset of the discovered terrestrial exoplanets will have system properties that make them amenable to follow-up observations to study their

costb001@ucr.edu

* 51 Pegasi b Postdoctoral Fellow

† UC Chancellor's Fellow

atmospheres (Morley et al. 2017; Batalha et al. 2018; Lincowski et al. 2019; Lustig-Yaeger et al. 2019). These atmospheric studies are crucial for ascertaining the true nature of the planetary surface properties and its evolutionary pathway. A direct comparison is generally made to our local analog of Venus, whose differing atmospheric evolution from Earth has been the subject of considerable amounts of research effort (Donahue et al. 1982; Kasting 1988; Hamano et al. 2013; Way et al. 2016; Kane et al. 2019; Way & Del Genio 2020; Turbet et al. 2021). This research can be furthered by studying Earth-like and Venus-like exoplanets to identify whether incident flux is primarily responsible for the climate divergence of Venus, or if it is due to other factors, such as planet size, degassing rates, and atmospheric loss.

Atmospheric spectroscopy is likely to produce the most robust diagnostic that can distinguish between the various exoVenus scenarios (Ehrenreich et al. 2012; Barstow et al. 2016), and various methods have been developed to predict the potential signal-to-noise of transmission spectroscopy observations (Kempton et al. 2018; Ostberg & Kane 2019). With a vast array of exoplanet targets now available, and coupled with limited follow-up opportunities, the prioritization of terrestrial targets is becoming increasingly important. Categorizing the known planets as lying in the Habitable Zone (HZ) of their host star (Kasting et al. 1993; Kopparapu et al. 2013, 2014), the region around a star where surface water may be present on terrestrial planets given sufficient atmospheric pressure, is an effective means to creating such a prioritization scheme, with a focus on potential Earth analogs. To aid in these efforts, various catalogs of HZ planets have been constructed (Hill et al. 2023), including those based on Hipparcos data (Chandler et al. 2016), Kepler discoveries (Kane et al. 2016), and the TESS observational strategy (Kaltenegger et al. 2019). Given the intrinsic biases of exoplanet detection methods toward close-in planets, many more exoplanets lie within the Venus Zone (VZ) of their system, defined as the region around a star interior to the runaway greenhouse boundary, and thus where terrestrial planets may be Venus analogs in a post runaway greenhouse state (Kane et al. 2014).

In the near-term, the primary method for studying the atmospheric composition of Venus-like worlds will be through transmission spectroscopy, which is used to determine the wavelengths at which light is absorbed when passing through a planet’s atmosphere. Venus’ transmission spectrum was modeled in preparation for Venus’ stellar occultation in 2012, which demonstrated that the Venusian cloud and haze layers prevent transmission spectroscopy from probing the atmosphere be-

low an altitude of 80 km (Ehrenreich et al. 2012). The effect of clouds on Venus’ transmission spectrum was also shown to cause difficulties for retrieval algorithms that were unable to consistently differentiate Earth and Venus-like atmospheres (Barstow et al. 2016). Lincowski et al. (2018) modeled the transmission spectra of the TRAPPIST-1 planets assuming they had 10-bar Venus-like atmospheres. Their work illustrated that the weaker CO₂ absorption bands at 1.05 and 1.3 μm and absorption caused by sulfuric acid clouds are likely to be the best avenues for determining if a planet has Venus-like surface conditions. Simulated JWST observations of the TRAPPIST-1 planets with Venus-like atmospheres showed that their atmospheres could be detected in less than 20 transit observations, but discerning their compositions would take more than 60 transit observations (Lustig-Yaeger et al. 2019). The catalog and selection criteria provided in this work will help to guide the identification of VZ planets for atmospheric follow-up observations to test atmospheric evolution scenarios.

Here, we present the results of a compilation and analysis of VZ candidates from the known inventory of exoplanets. The purpose of the VZ catalog is to study the demographics of terrestrial planets that lie within the VZ, and to facilitate the prioritization of follow-up targets whose atmospheric characterization will provide critical diagnostics in determining the inner edge of the HZ. Section 2 describes the extraction and parsing of exoplanet data, the radius constraints used to identify terrestrial planets, and the calculations that allow the analyses of the bulk data characteristics. The creation of an extensive table of terrestrial planets whose orbits lie partially or wholly within the VZ is presented in Section 3. In Section 4, we provide a discussion of the VZ population demographics and highlight potential priority for James Webb Space Telescope (JWST) targets, as well as other important follow-up opportunities. Since the catalog includes both transiting and non-transiting exoplanets, we further discuss the importance of non-transiting targets for future studies of terrestrial planet evolution. Section 5 includes a summary of the main results, concluding remarks, and an outline of further potential uses of the VZ catalog.

2. DATA EXTRACTION AND CALCULATIONS

We define terrestrial VZ planets to be planets with radii $R_p < 2.0 R_\oplus$ that spend any portion of their orbits within the boundaries of the VZ. Note that the radius limit for terrestrial planets depends on numerous factors, including formation scenarios and composition (Unterborn & Panero 2019), and not all planets within this range will indeed be rocky (Rogers 2015). However,

this radius cutoff was chosen to account for uncertainties in radius measurements or calculations to minimize the exclusion of any terrestrial planets from the sample. Terrestrial VZ planets with measured radii have an average uncertainty of $0.2 R_{\oplus}$, while the maximum uncertainty is as high as $1.03 R_{\oplus}$. Planets with radii $R_p > 2.0 R_{\oplus}$ and relatively high or low mass likely require significant Fe-enrichment relative to their host star or surface volatiles to explain their anomalously higher or lower than expected density. These planets would therefore be more likely to be super-Mercuries or volatile-rich mini-Neptunes/water worlds, respectively (Unterborn et al. 2016; Unterborn & Panero 2019).

The inner boundary of the VZ is defined as $25 \times$ the incident flux received by Earth (F_{\oplus}), which is the insolation flux limit where Venus would begin to lose the majority of its atmosphere (Zahnle & Catling 2017). Note that this does not account for variations in stellar activity as a function of spectral type, but is broadly encapsulating the vast range of expected stellar ages and masses, as well as planetary masses and atmospheres, expected to lie within our sample. The outer VZ boundary is the runaway greenhouse boundary, which corresponds to the inner boundary of the conservative HZ (CHZ), and is defined as the insolation flux threshold where liquid water on Earth's surface would be evaporated, forcing it into a runaway greenhouse state (Kopparapu et al. 2013, 2014). To determine whether a planet orbits within the VZ we used Kepler's equation to calculate the planet's distance from its host star as a function of its orbit. If a planet's distance is ever less than the distance of the outer VZ boundary and greater than the distance of the inner VZ boundary, then the planet orbits within the VZ. The 317 known terrestrial planets from the NEA that spend any amount of their orbit in the VZ (hereafter referred to as VZ terrestrial planets) are shown in Figure 1. It should be noted that planets within the VZ are not guaranteed to have Venus-like surface conditions. The VZ is instead a first-order estimate for identifying planets that may be Venus-like and for guiding target selection for follow-up observations with JWST or other future facilities. These observations will be the primary method of producing more accurate predictions of the surface conditions of VZ planets.

The possibility of habitable worlds within the VZ cannot be discounted either, as it has been shown that Venus could have maintained temperate surface conditions for as recently as 1 Gya (Way & Del Genio 2020). However, this scenario requires a young Venus to be cool enough to allow water to condense on its surface, which faces challenges due to the possible lack of cloud formation at the substellar point (Turbet et al. 2021). At-

mospheric spectroscopy of terrestrial planets in the VZ will be essential for investigating both the possibility of a temperate period in Venus' history, and the conditions that force a planet into a runaway greenhouse. Furthermore, terrestrial planets have long been known to differ significantly in their geologic (Head et al. 1977) and tectonic evolution (Head & Solomon 1981), and their mechanisms of global lithospheric heat transfer and loss (Head et al. 1981) suggested the presence of ongoing global plate tectonics (Head III & Crumpler 1987), a hypothesis tested by the Magellan mission. Magellan data revealed a geologically very young surface (~ 1 Gyr; McKinnon et al. 1997) and a single global lithospheric plate lacking a system of ongoing plate tectonics (Solomon et al. 1991, 1992). Similarly, the currently observed atmosphere of Venus may have formed relatively recently geologically, transitioning from Earth-like oceanic conditions (Way & Del Genio 2020) (the ‘great climate transition’) during the early stages (Byrne et al. 2021) of the young remnant surface geological record (Ivanov & Papaloizou 2011), or in an additive manner throughout this period (Khawja et al. 2020). Alternatively, the current Venus atmosphere may be a “fossil atmosphere” dating from some time earlier in the history of Venus (Head et al. 2021). Indeed, the conundrum of the Earth-Venus relationship (Head 2014) is one of the most compelling outstanding scientific questions today. As we explore both forward models and inverse models to understand the nature, origin and evolution of the Venus atmosphere, the greatly enlarged exploratory parameter space provided by the demographics of terrestrial exoplanets in the Venus Zone is designed to contribute a much needed broader perspective on the problem, and a guide to obtaining the most critical observations to improve our understanding.

All of the planetary and stellar data used in this work were acquired from the NASA Exoplanet Archive (NEA; Akeson et al. 2013) using the Application Program Interface (API). We used the default properties for each system, and the data are current as of 2023 January 19 (NASA Exoplanet Archive 2023). Each planetary system was required to have non-null values for the host star effective temperature and the planetary semi-major axis, or the means to calculate it, else it was removed from the sample. If orbital eccentricity was not measured for a planet, the orbit was assumed to be circular, while the argument of periastron was set to 90° if no value was available. The majority of VZ planets have an orbital eccentricity of 0, with 76% of them having no measured eccentricity which were then assumed to be 0, while 6% of planets were observed to have 0 eccentricity. The remaining planets all had non-zero eccen-

tricities. Assuming circular orbits may have excluded planets which would enter the VZ with eccentric orbits, however we expect this to have a negligible effect on the total amount of terrestrial VZ planets. This assumption planets beyond the outer VZ boundary, however a circular orbit is the appropriate assumption for planets between the inner VZ boundary and the host star because of the likelihood of tidal locking.

If not available for a given system, the values for stellar luminosity, planet incident flux, and planet equilibrium temperature were calculated when possible. If either a measured planet radius or mass were not available, then the missing values were calculated using the methodology of [Chen & Kipping \(2017\)](#). Due to the restraints of mass-radius relationship, radius calculations were limited to planets with mass $M_p < 25 M_{\oplus}$, while mass calculations required planet radius $R_p < 5 R_{\oplus}$. We did not incorporate the uncertainties when calculating the mass or radius using the [Chen & Kipping \(2017\)](#) method. The estimated RV amplitude for each planet was calculated when possible, using equations 12–14 from [Lovis et al. \(2010\)](#). If the semi-major axis of the planet was not available, it was calculated from the orbital period and stellar mass.

3. A CATALOG OF VZ EXOPLANETS

Here we present the data for all known VZ planets that were identified using the methodology described in Section 2. These results are shown in Table 1, where the data are listed in alphabetical order based on the planet names. The percentage of a planet’s orbit that is spent within the VZ and CHZ are shown in the columns labeled ‘VZ (%)’ and ‘CHZ (%)’, respectively. If a planet does not spend 100% of its orbit in the VZ, then it will spend the remainder of its orbit in either the CHZ, or between the inner VZ boundary and the host star. Thus, the summation of the CHZ and VZ columns will generally constitute 100% of the orbit, except in cases where the planet ventures interior to the inner VZ boundary.

The location column, marked ‘Loc’, indicates where the relative location of the planet’s semi-major axis, a , lies within the VZ. The location values range from 0–1, where 0 is the inner VZ boundary and 1 is the outer VZ boundary. Planetary radii (R_p) and masses (M_p) are included in the table, with italicized values representing those that were calculated using the [Chen & Kipping \(2017\)](#) mass-radius relationship. Orbital period, P , semi-major axis, a , planetary equilibrium temperature, T_{eq} , and RV amplitude, K , are included for each planet when available. We included the calculated transmission spectroscopy metric (TSM) value for each planet using the methods of [Kempton et al. \(2018\)](#). The TSM

is used to estimate the achievable signal-to-noise ratio (S/N) of transmission spectroscopy with JWST assuming 10 hours of observations. In this work we do not focus on the magnitude of individual TSM values, but instead on TSM values in reference to each other. In general, we view the planets with the largest TSM values compared to other planets in the sample as having the most potential for success in follow-up observations. The orbital eccentricity, e , of a planet was set to 0 when no eccentricity measurement was available, which are listed as a single italicized 0 in the table. Measured eccentricities of 0 are listed as ‘0.000’.

Table 2 includes details for each VZ planet’s host star. R_{\star} and M_{\star} are the radius and mass of the star in solar units, respectively. Jmag and Vmag are the J-band and V-band magnitude of the star, respectively. The stellar effective temperature, T_{eff} , surface gravity, $\log g$, luminosity, L_{\star} , and distance, d , of the stars are also shown in Table 2. In the case of the NEA providing null values for L_{\star} , we calculated L_{\star} using R_{\star} and T_{eff} when they are available.

4. DISCUSSION

4.1. Demographics

Unveiling the demographics of various planet populations provides insight into planet formation and evolution scenarios, which are particularly important for the potential creation of runaway greenhouse planets. Figure 2 presents property distributions for the planets in our sample, including orbital eccentricity (upper left), orbital period (upper right), planet radius (lower left), and planet mass (lower right). The shown distributions compare the VZ terrestrial planets (yellow) with all terrestrial planets (blue) and the general planet population (black). For the VZ terrestrial (yellow) and all terrestrial (blue) populations, the period distribution is remarkably gaussian (at least in log space), such that the distribution peaks approximately at the mean value. However, this is not true of the general planet population, which is rather asymmetric due to inclusion of cold giant planets. Interesting to note that the orbital period limit of the terrestrial planet distribution approximately coincides with the outer edge of the VZ. This is due to planet detection missions being biased towards closer in planets which has resulted in the discovery of only 29 terrestrial planets with orbits beyond the outer VZ boundary ([Hill et al. 2023](#)). The planet radius and mass histograms compare VZ planets of all radii to all known exoplanets. A radius gap is visible in both the VZ and all planet distributions (e.g. [Lopez & Fortney 2013](#); [Owen & Wu 2013](#); [Fulton et al. 2017](#)), with a sharp cutoff of VZ planets at $\sim 14 R_{\oplus}$. The cutoff

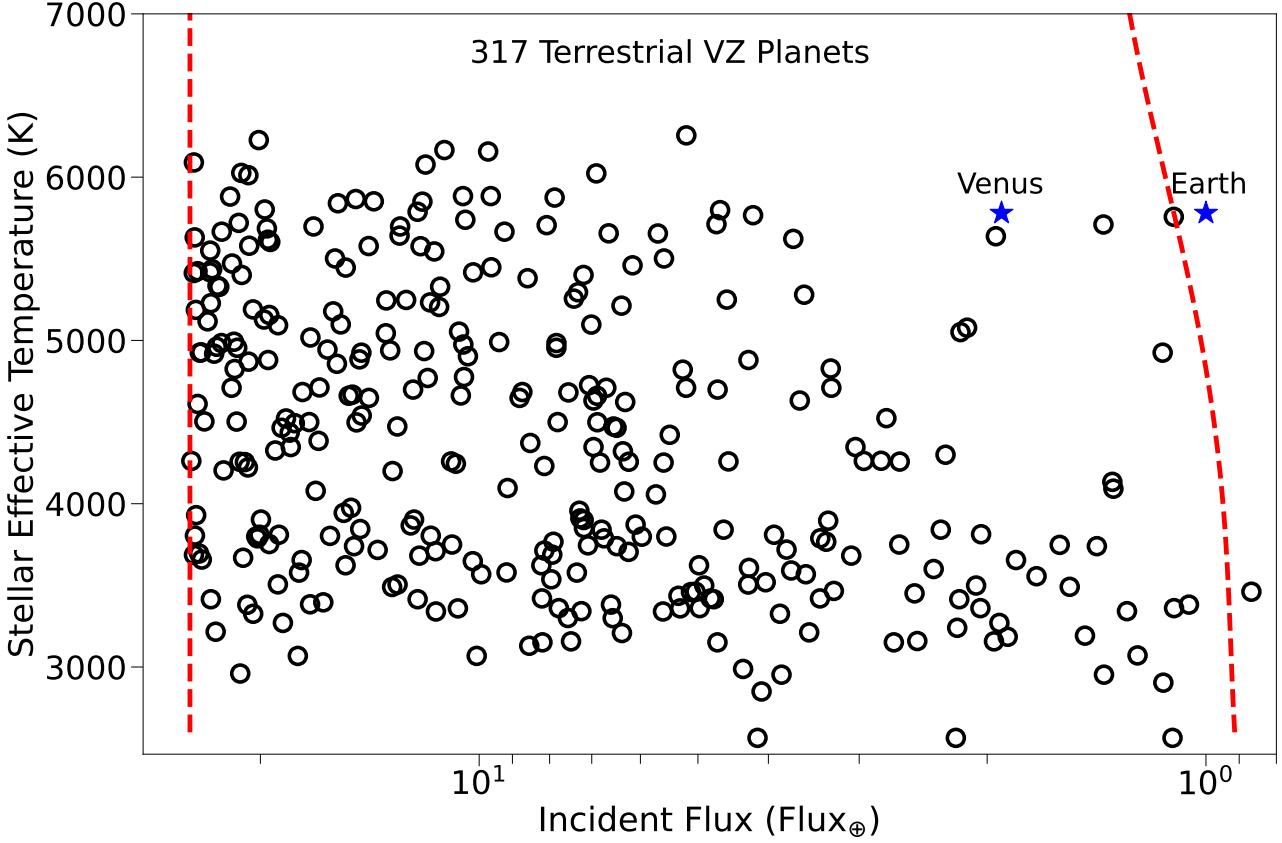


Figure 1. Terrestrial planets from the NEA that spend any part of their orbit in the VZ. The inner VZ boundary is indicated by the left line, and the right line is the outer VZ boundary. Earth and Venus are shown for reference (blue stars).

is present because the gravitational force of high mass planets typically prevents their size from exceeding $\approx 14 R_{\oplus}$. Exceptional cases such as hot-Jupiters can exceed this limit because their atmospheres puff up from high insolation flux, however these planets are too close to their stars to be in the VZ.

Host star properties such as T_{eff} (upper left), $\log g$ (upper right), Jmag (lower left), and stellar distance (lower right) are displayed in Figure 3. All plots compare the host stars of VZ terrestrial planets to those of all terrestrial planets, and all planets regardless of their size. Terrestrial VZ planets (yellow) are most commonly found around cooler, smaller stars where the sensitivity of observations toward terrestrial planets is greater, and is thus likely related to an observational bias. By contrast, the two other subsets (black and blue) have been more commonly detected around hotter, brighter Sun-like stars that are better suited for RV observations. Similarly, the dependence of the respective detected planet populations on $\log g$ demonstrates that the terrestrial planets, including those in the VZ, are overwhelmingly found around main sequence stars, whose relatively small size enable the detection of pro-

portionally small planets. Furthermore, the majority of exoplanets have been found around fainter stars, with the distribution of host star J-band magnitudes peaking at ~ 13 . Note that the J-band magnitude distribution for the sample that includes all exoplanet host stars has an additional peak at ~ 7 , largely due to the effect of RV surveys that target preferentially brighter stars than those included in transit surveys. The bottom-right panel of Figure 3 shows the distribution of stellar distances for the respective samples, where the number of known planets naturally rises with increasing distance due to the volume limited nature of the various exoplanet surveys. Note also the indication of the nearest exoplanet, Proxima Centauri b, at the far left of the figure; a non-transiting exoVenus candidate (see Section 4.4).

Figure 4 displays relationships between various parameters for terrestrial VZ planets compared to all known planets. The upper left figure shows planet mass versus planet radius. Since most VZ planets lack either a radius and mass measurement, the trend seen is representative of the mass-radius relationship that was used to calculate the missing mass or radius values (Chen &

Kipping 2017). The upper right figure displays orbital period vs orbital eccentricity for all planets with non-zero eccentricities. Few VZ planets are displayed since the majority did not have measured eccentricities. The lower left plot displays orbital period vs planet mass and the lower right shows orbital period vs planet radius. The upper limit planet radius set for our VZ sample can be seen in the lower right plot. Similarly, there is a cut-off in mass in the lower left plot caused by how most masses were calculated using the mass-radius relationship. There is an additional radius cutoff for all known planets around $10 R_{\oplus}$ which is also caused by the mass-radius relationship. The relationship plateaus at higher planet mass and radius as demonstrated in the upper left plot.

4.2. JWST VZ Targets

Observations of exoplanet atmospheres will provide information that is necessary for understanding their climates. During Cycle 1, JWST will conduct such observations for eight terrestrial VZ planets: GJ 357 b (Luque et al. 2019), GJ 1132 b (Bonfils et al. 2018), TRAPPIST-1 b (Agol et al. 2021), TRAPPIST-1 c (Agol et al. 2021), TOI-776 b (Luque et al. 2021), TOI-776 c (Luque et al. 2021), LTT 1145 A b (Winters et al. 2022), and L 98-59 b (Demangeon et al. 2021). TOI-776 c has a radius of $2.02 R_{\oplus}$, but is within the upper radius limit for terrestrial planets when considering uncertainties. All of these planets will be observed with either the Mid-Infrared Instrument (MIRI; Wright et al. 2004), Near-Infrared Spectrograph (NIRSpec; Bagnasco et al. 2007), or the Near-Infrared Slitless Spectrograph (NIRISS; Doyon et al. 2012) aboard JWST. MIRI will be primarily used to observe the emission spectra of exoplanets, while NIRISS and NIRSpec will conduct transmission spectroscopy.

TOI-776 b, TOI-776 c, and L 98-59 b have the 3 highest TSM values among the VZ JWST targets. However, they are in close vicinity to the inner VZ boundary, which may have led to significant atmospheric loss (Van Eylen et al. 2018). TOI-776 b and TRAPPIST-1 c VZ planets are intriguing as they both have additional terrestrial VZ planets within their respective systems. TOI-776 b is accompanied by TOI-776 c, and TRAPPIST-1 c, b and d are all in the VZ. Atmospheric spectroscopy of multiple VZ planets within the same system offers the opportunity to investigate how VZ planet evolution may vary based on location in the VZ. Furthermore, the TRAPPIST-1 VZ planets will also be useful for comparison to their neighboring planets in the conservative HZ, TRAPPIST-1 e, f and g. Transmission or emission spectroscopy of VZ and HZ exoplanets in the

same system would be a unique opportunity to investigate evolutionary differences between Earth and Venus using exoplanets. TRAPPIST-1 c will receive 6 transit and 4 eclipse observations, while TRAPPIST-1 b, TOI-776 b, and TOI-776 c will each receive 2 transit observations.

GJ 357 b has a radius of $1.22 R_{\oplus}$ and is located 0.01 AU (Loc = 0.093) from the inner VZ boundary. The close proximity to its host star causes GJ 357 b to experience and incident flux of $\sim 13 F_{\oplus}$, placing it at risk of sustaining significant atmospheric loss. Transmission spectroscopy of the planet will aid in determining the presence of an atmosphere and, in turn, be a useful test for the location of the inner VZ boundary. GJ 357 b will be observed for a single transit by JWST NIRSpec during Cycle 1 observations. GJ 1132 b is also located close to the inner VZ boundary, and its eccentric orbit results in it spending 23% of the orbit between the inner VZ boundary and its host star. It has a radius of $1.13 R_{\oplus}$, making it also susceptible to substantial atmospheric loss and a useful test for the location of the inner VZ boundary as well. GJ 1132 b is anticipated to have two transit observed by JWST NIRSpec during Cycle 1.

LTT 1145 A b orbits a single star but is in an M-dwarf triple binary system with LTT 1145 BC. The system the planet is in makes it unique from the other VZ planets being observed by JWST, however since LTT 1145 BC are 34 AU from LTT 1145 A, it is unlikely that they have any significant contribution to the energy budget of LTT 1145 A b. There are two sets of observations planned for LTT 1145 A b, with a single transit observation by JWST NIRSpec and three secondary eclipse observations by JWST MIRI. Additional observations of its neighboring terrestrial planet in the VZ would illustrate whether their differences in received flux resulted in different climates.

L 98-59 b spends 63% of its orbit in the VZ, and the rest between the inner VZ boundary and its host star. Throughout its eccentric orbit the planet receives stellar flux that varies from $19-29 F_{\oplus}$. The likelihood that the planet has sustained significant atmospheric loss is increased by both its high incident flux and smaller size of $0.85 R_{\oplus}$. Two transit observations with JWST NIRSpec are planned for the planet, and detection of an atmosphere on this planet would demonstrate that VZ planets can sustain an atmosphere closer to the star than predicted by the inner VZ boundary. Besides L 98-59 b, there are 3 other terrestrial planets in its system that are also in the VZ. Observations of all planets in the system would be valuable for understanding the runaway greenhouse effect across a range of planet scenarios for the same host star.

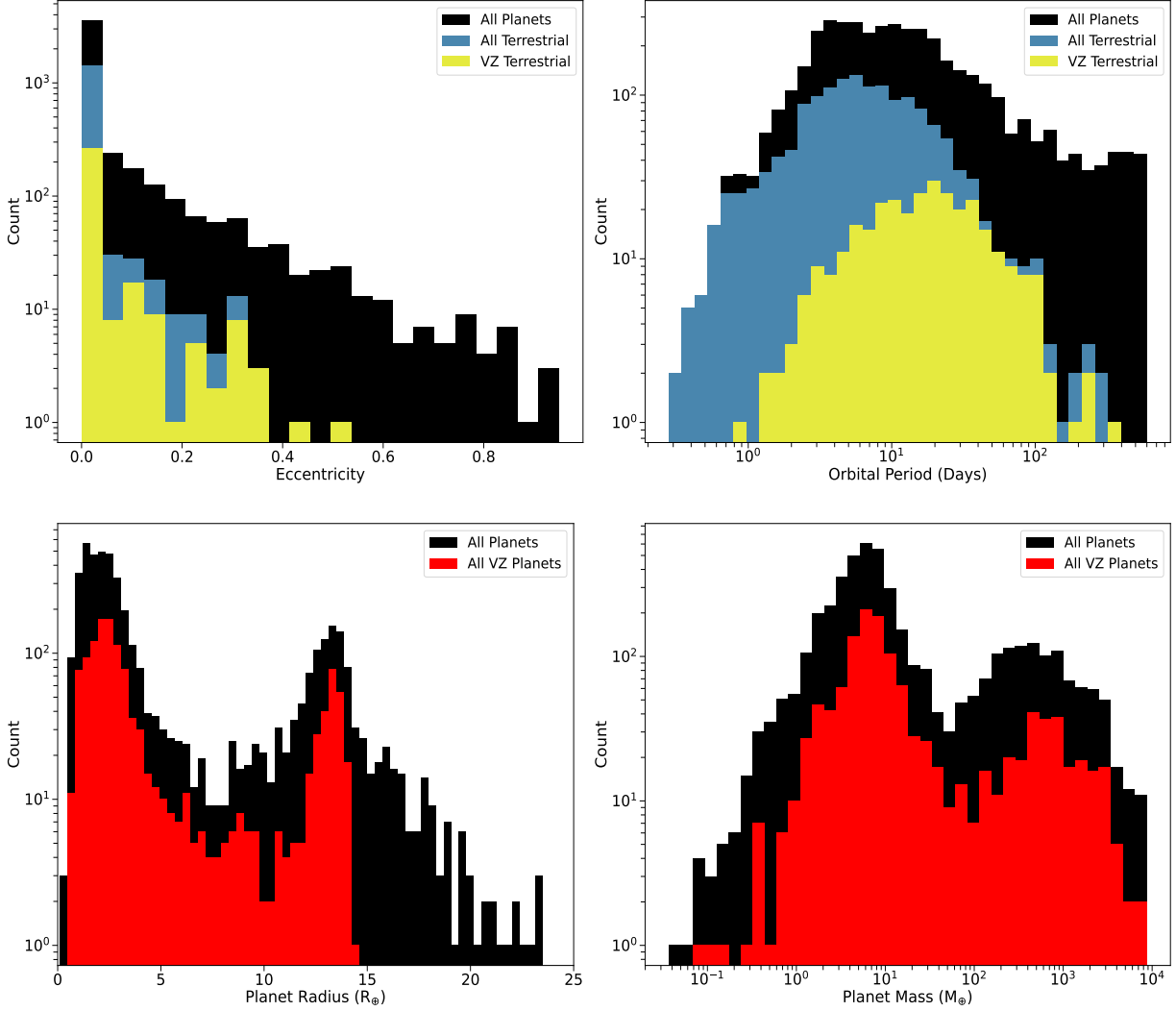


Figure 2. Histograms illustrating the distribution of orbital eccentricity (upper left), orbital period (upper right), planet radius (bottom left), and planet mass (bottom right). In the upper two plots, the yellow distribution indicates terrestrial VZ planets and the blue distribution is all known terrestrial planets. In the bottom two plots the red distribution is all known planets within the VZ, regardless of their size. In all four plots the black distribution is all known planets regardless of radius or location.

The success of these observations will be highly dependent on the planets' atmospheres. If they were to have Venus-like atmospheres, then it is likely that JWST will be unable to detect any molecular species in their transmission spectra given the allotted observation time, but may still be able to determine the presence of an atmosphere. If the planets have Earth-like or oxygen-desiccated atmospheres, then detecting molecules in their atmospheres may be achieved in as little as 6 transits (Lustig-Yaeger et al. 2019; Pidhorodetska et al. 2021).

4.3. VZ Targets for Future Observations

Here we highlight the VZ planets with high scientific value which are the most amenable to atmospheric spec-

troscopy and should be considered for observations in JWST Cycle 2+ or by other future facilities. All planets we considered were required to be known to transit, and the TSM value was used as the basis for quantifying the observational potential of planets. A high equilibrium temperature can cause a planet to have a high TSM value, but planets closer to the outer VZ boundary maximize similarities between the planets and Venus. Figure 5 displays the VZ location and radii of VZ planets, with points colored based on their TSM value. Based on our selection criteria, an optimal planet would be at $0.95 R_{\oplus}$, at the far right of the figure, and colored yellow. There is a scarcity of planets in that region, and therefore no planets that exactly match our criteria. Hence, we handpicked the planets we deemed to have the best

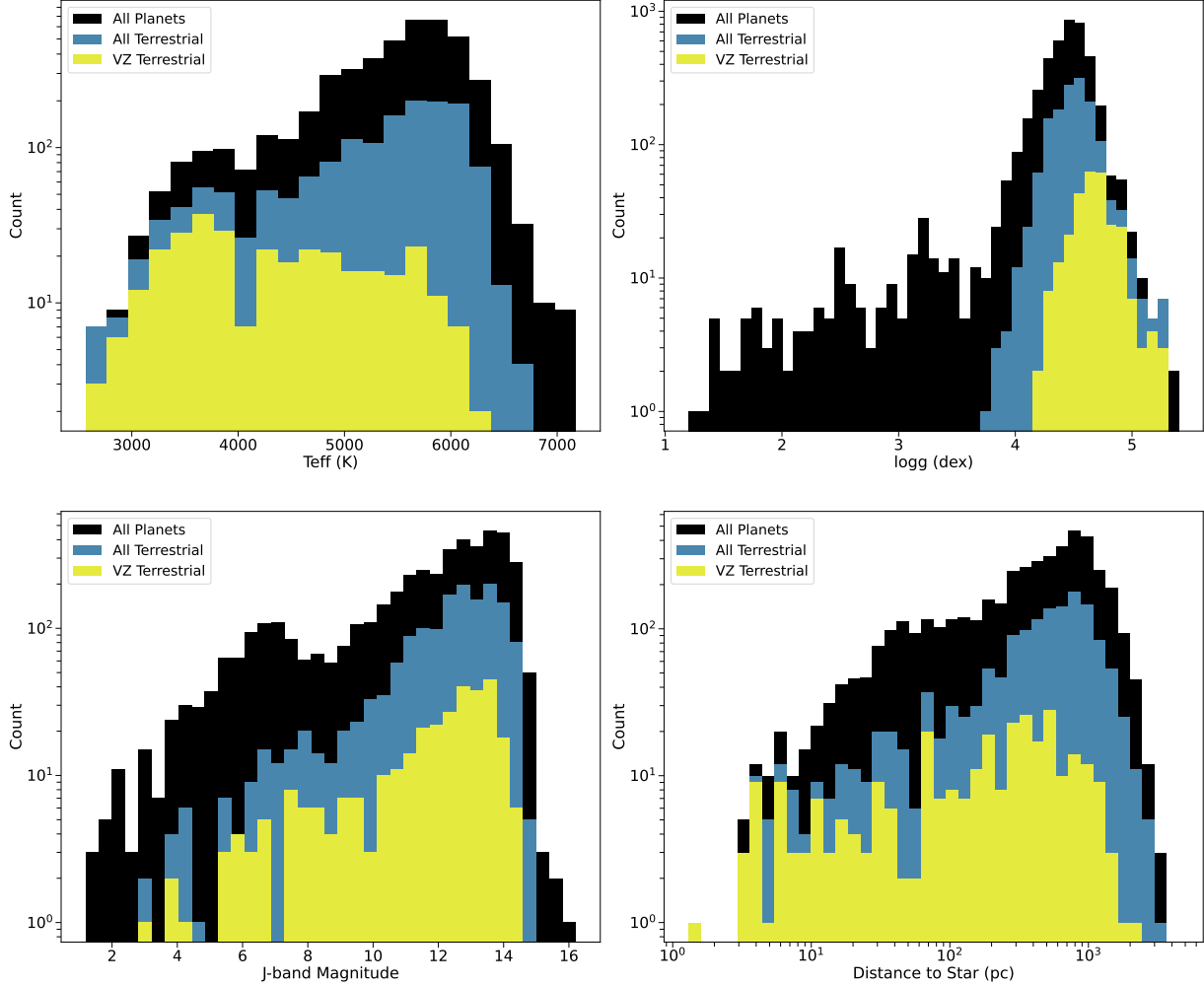


Figure 3. Histograms displaying distributions of stellar properties: stellar effective temperature (upper left), surface gravity (upper right), J-band magnitude (bottom left), distance to star (bottom right). In yellow is the distribution for the host stars of terrestrial VZ planets, in blue is the host stars of all terrestrial planets, and the black distribution is all known planets regardless of size or location.

combination of observation potential, size similarity to Venus, and general scientific promise. The five planets we determined to have the best combination of scientific intrigue and observational amenability are TOI-2285 b (Fukui et al. 2022), LTT 1445 A c (Winters et al. 2022), TOI-1266 c (Demory et al. 2020), LHS 1140 c (Lillo-Box et al. 2020), and L 98-59 d (Demangeon et al. 2021).

TOI-2285 b is the only planet of the six that spends a portion (12%) of its orbit in the CHZ due to its orbital eccentricity of 0.3. The TSM of this planet is the second lowest of the group, but its orbit makes it an interesting test case for the climate of a planet in both the VZ and HZ. Out of the 6 planets, LTT 1445 A c is the closest in size and mass to that of Venus, with a measured radius and mass of $1.14 R_{\oplus}$ and $1.54 M_{\oplus}$, respectively. The planet orbits a single star in an M-dwarf triple binary with LTT 1445 BC and has a TSM of 45, which is the

third highest of the group. TOI-1266 c is in the center of the VZ, and has the second highest TSM value of the six targets. It has a measured radius of $1.55 R_{\oplus}$ and a measured mass of $2.2 M_{\oplus}$, making it considerably larger and more massive than Venus. Observing its atmosphere would help determine whether the surface conditions of more massive planets in the VZ differ from those closer to Venus in size. In addition, the detection or non-detection of an atmosphere on TOI-1266 c would help justify the location of the inner VZ boundary by illustrating whether planets more massive than Venus can sustain an atmosphere despite having a higher equilibrium temperature and orbiting a highly active M-dwarf star.

LHS 1140 c is the second most similar to Venus in size from the six future targets, with a measured radius of $1.16 R_{\oplus}$. The planet orbits an ultra-cool red-dwarf, but

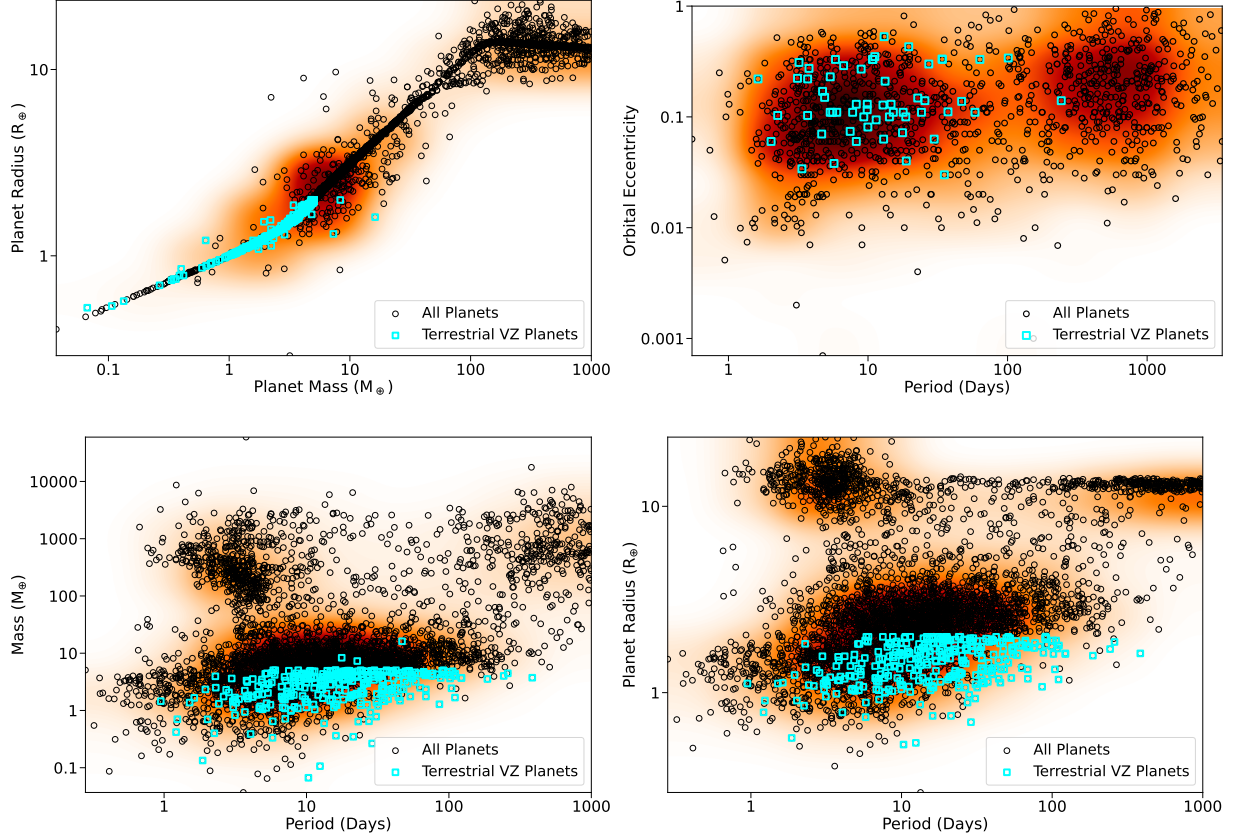


Figure 4. The relationships between various planet properties. In all plots, the black circles are all known planets regardless of size or location while the blue squares are terrestrial VZ planets.

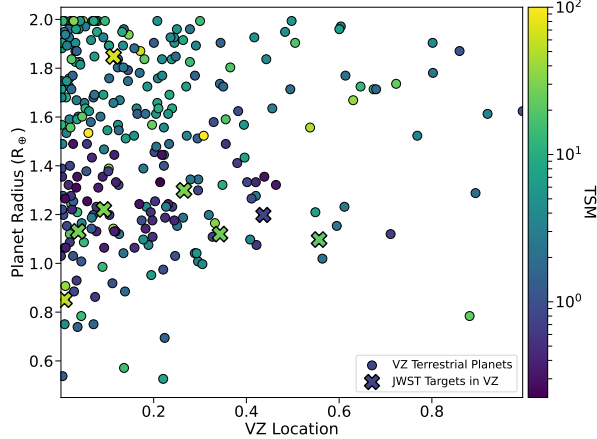


Figure 5. Terrestrial VZ planets colored based on their TSM value. The x-axis represents the planets' location in the VZ, where 1 indicates the outer VZ boundary and 0 is the inner VZ boundary. Data points denoted by an 'x' are VZ planets that are planned to be observed by JWST.

its orbital period of 3.7 days results in an incident flux of $4.3 F_{\oplus}$ and an equilibrium temperature of 709 K, which is the hottest of the group. Determining whether the planet has an atmosphere would help inform the atmo-

spheric escape experienced by Earth-sized VZ planets with high incident flux, which will test the location of the inner VZ boundary.

L 98-59 d is in a heavily populated VZ with three other terrestrial planets. Planet d was chosen from this system as it is the farthest planet from the inner VZ boundary that is also known to transit. L 98-59 d has by far the largest TSM value in the group and the third highest TSM value of all VZ planets. The large amount of VZ planets and their amenability to atmospheric spectroscopy make the L 98-59 system an important benchmark for studying the VZ.

The high priority targets of particular interest are those that have a neighboring terrestrial planet or planets in the VZ or HZ. LTT 1445 A c has a single terrestrial neighbor in the VZ that is planned to be observed by JWST, while L 98-59 d has three neighboring VZ planets, one of which will be observed by JWST. Currently the VZ only provides a general estimate for the climates of terrestrial planets, but observations of multiple VZ planets within the same system can be used to study the evolutionary differences of planets in the inner and outer VZ of the same system. LHS 1140 c is the only

planet in the group with a neighboring terrestrial planet in the HZ. Observations of both LHS 1140 c and b provide a chance to compare the differences between Earth and Venus to planets in a similar system.

4.4. Non-Transiting Planets of Interest

Limiting terrestrial VZ targets to those that are known to transit excludes 37 planets that may be useful for testing the VZ boundaries and studying evolutionary pathways of VZ planets. The atmospheres of these planets will be inaccessible to JWST, but a concept mission named the Mid Infrared Exoplanet CLimate Explorer (MIRECLE; Mandell et al. 2022) would use thermal emission to constrain the surface temperature and atmospheric composition of non-transiting rocky exoplanets. Although MIRECLE is currently a concept, it is valuable to identify which non-transiting VZ planets would be beneficial for studying Venus and the VZ. Non-transiting planet candidates were chosen based on their vicinity to the outer VZ boundary, similarity in size to Venus, and Emission Spectroscopy Metric (ESM; Kempton et al. 2018) value at both 7.5 and 15 μm (Figure 6). Similar to TSM, ESM values provide a first-order S/N estimate of the emission spectrum of a planet. A more detailed explanation of both the TSM and ESM can be found in Kempton et al. (2018). Using these criteria we chose six planets: GJ 3323 b (Astudillo-Defru et al. 2017); GJ 1061 b, GJ 1061 c, and GJ 1061 d (Dreizler et al. 2020); Proxima Centauri b (Anglada-Escudé et al. 2016); and Teegarden’s Star b (Zechmeister et al. 2019).

GJ 3323 b has ESM values of 10.1 and 56.0 at 7.5 and 15 μm , respectively. These ESM values are the second highest among all non-transiting, terrestrial VZ planets. Its orbit places it at roughly the center of the VZ, and it has a measured mass and estimated radius of 2.02 M_{\oplus} and 1.25 R_{\oplus} , respectively. The planet is a good test case to study the runaway greenhouse limit for more massive planets.

Proxima Centauri b has a measured mass of 1.27 M_{\oplus} , an estimated radius of 1.05 R_{\oplus} , and an orbital eccentricity of ~ 0.35 (Bixel & Apai 2017; Kane et al. 2017). Its eccentric orbit causes it to spend 75% of its orbit in the HZ and 25% in the VZ, during which it receives varying incident flux that ranges from 0.36–1.55 F_{\oplus} . Studying the planet is valuable for determining whether its short exposure to higher insolation flux was sufficient enough to force it into a runaway greenhouse. This will also inherently be a test for the climate evolution of planets with eccentric orbits that straddle the runaway greenhouse boundary. Its ESM value of 33.3 at 15 μm makes it a strong candidate for observations with emission spectroscopy.

Teegarden’s Star b is physically similar to Earth as well, with a measured mass and estimated radius of 1.05 M_{\oplus} and 1.02 R_{\oplus} , respectively. It has an ESM value of 18.8 at 15 μm , which is second lowest of the 6 non-transiting planets we chose. The planet spends all of its orbit within VZ and is only 0.03 AU from the outer VZ boundary, which makes it an excellent case for testing runaway greenhouse conditions. In addition, Teegarden’s Star was determined to have an age greater than 8 Gyr (Zechmeister et al. 2019), allowing for the opportunity to study any correlations between planet age and the onset of the runaway greenhouse effect (Foley & Smye 2018; Foley 2019; Unterborn et al. 2022).

The GJ 1061 system has three planets with eccentric orbits that all spend some portion of their orbits in the VZ. The orbit of GJ 1061 b has an eccentricity $e = 0.31$, and a semi-major axis in the inner half of the VZ ($\text{loc} = 0.36$). It has the highest equilibrium temperature among the GJ 1061 VZ planets, and therefore has the highest ESM of the 3 planets. GJ 1061 c spends 73% of its orbit within the VZ and the rest within the conservative HZ. Similarly, GJ 1061 d spends 22% of its orbit in the VZ and the rest in the conservative HZ. Given their orbits, GJ 1061 b and c both offer an opportunity to study the effect of varying insolation flux on a planet’s climate. However it should be noted that the eccentricity values reported for these planets are upper limits (Dreizler et al. 2020), and circular orbits would make planet c orbit within only the VZ, and planet d only in the HZ. Despite this, the system as a whole would be a useful sample of planetary atmospheres that span across the VZ of a single star.

4.5. Direct Imaging of Nearby Stars

Their intrinsic brightness and closer orbital distance from their host stars make VZ planets potentially interesting targets for the next generation space-based direct imaging (DI) missions, assuming those VZ planets have similar characteristics to that of Venus. Successful DI of an exoplanet requires the target planet to have planet-to-star flux ratios that are above the instrument’s minimum contrast ratio requirement at locations in the planet’s orbit where the planet-star angular separation is larger than the instrument’s inner working angle (IWA). In our estimate of the DI prospects of VZ planets around nearby stars, we assumed usage of the Habitable Exoplanet Observatory (HabEx) mission concept with an external starshade. The HabEx starshade has a required contrast ratio performance of 1×10^{-10} , and optimistically, 4×10^{-11} (Gaudi et al. 2020) at the IWA of 70 mas, which is the angular radius of the starshade itself as seen from the telescope in the visible channel. Typically,

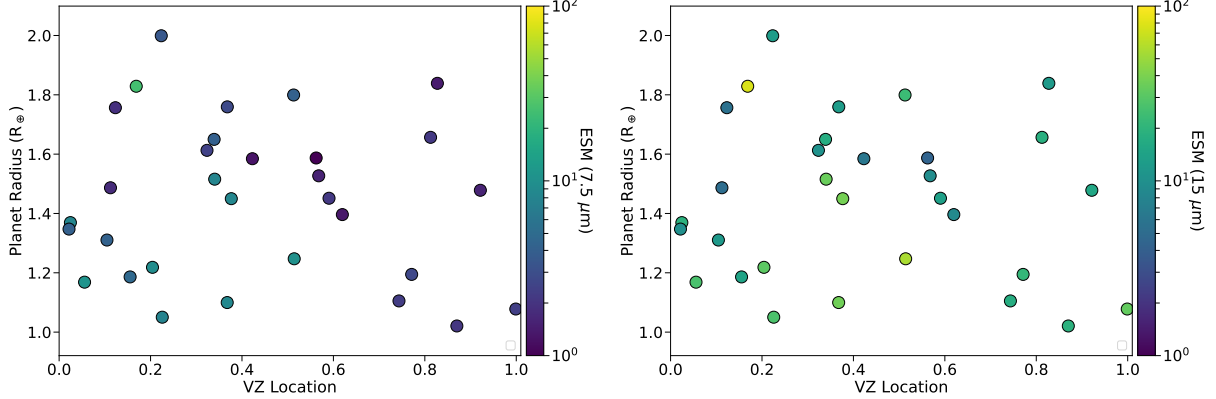


Figure 6. The ESM values of all non-transiting, terrestrial VZ planets at both $7.5\text{ }\mu\text{m}$ (left) and $15\text{ }\mu\text{m}$ (right).

planets that orbit inside the IWA of the instrument are considered undetectable due to the obstruction of the starshade. However, it has been demonstrated that this inner limit can be pushed further inward if taking into account the transmittance profile of the starshade itself (Gaudi et al. 2020; Li et al. 2021). For HabEx, such limit, which we refer to as $\text{IWA}_{0.5}$, is at angular separation of 56.4 mas from the center of the starshade where the starshade transmittance is only 0.5. Here, we employed the 56.4 mas of $\text{IWA}_{0.5}$ and the required 1×10^{-10} contrast threshold as the hard limit of HabEx visibility of VZ planets.

We first checked detectability of known VZ planets taking reported orbital parameters and distance to each star. None of the known VZ planets can be directly imaged owing to the small on-sky angular separation of those planets. Out of these known VZ planets, Proxima Cen b has the largest angular separation of 50 mas, which puts it just inside the HabEx $\text{IWA}_{0.5}$ limit of 56.4 mas. Next, we checked whether additional undiscovered VZ planets could be detected through direct imaging. We expanded our VZ planet DI detectability estimate to nearby stars within 30 pc. We queried the Gaia Data Release 3 (DR3) database (Gaia Collaboration et al. 2022) and collected all stars within 30 pc with effective temperatures between 2500 K and 7500 K. In total, 3814 nearby stars were collected.

For each star, we calculated the angular separation of the runaway greenhouse boundary (Kopparapu et al. 2013, 2014) based on the distance, stellar radius, and effective temperature values from Gaia DR 3. We injected one fictitious VZ planet with 1 Earth radius at the runaway greenhouse boundary around each star with circular face-on orbit and assumed a geometric albedo similar to that of Venus from the Haystacks modern solar system model, which is 0.6 (Roberge et al. 2017). Following Li et al. (2021), we estimated flux ratio varia-

tion along the entire orbit for each fictitious planet and determined the maximum planet-to-star flux ratio of the fictitious planet while being outside the $\text{IWA}_{0.5}$. In the case of face-on inclination angles, flux ratios of planets are constant since they have the same phase throughout their entire orbit. The planet detectability based on flux ratios were only estimated to the first order. That is, no noise sources such as sky noise, residual starlight from imperfect starshade, clock-induced-charge etc. were included in the estimation. We show the result in Figure 7, where the maximum angular separations of fictitious VZ planets are plotted against their distances from Earth to their host stars. Each individual point in the figure represents one fictitious VZ planet orbiting at the runaway greenhouse boundary around one of the nearby stars. Points are color coded based on the planets' maximum flux ratios at any point throughout their entire orbits. VZ planets that are greyed out are therefore undetectable at any orbital locations under our DI setup. Planets that have maximum angular separations smaller than $\text{IWA}_{0.5}$ of 56.4 mas or have maximum flux ratios below the instrument minimum contrast threshold of 1×10^{-10} are indicated by grey points. The two red horizontal lines represent the angular sizes of HabEx starshade IWA and $\text{IWA}_{0.5}$.

As can be seen in Figure 7, there exhibits a clear downward trend in terms of VZ planets detectability as a function of angular separation. The number of potentially detectable VZ planets around nearby stars quickly diminishes towards the 30 pc distance mark. This is because at larger distances, most VZ planets at the runaway greenhouse boundaries extends smaller than $\text{IWA}_{0.5}$ angular separations from their host stars, thus blocked by the starshade. For a few fictitious VZ planets that have large angular separation at large distances (top right corner of Figure 7), high stellar effective temperatures push the runaway greenhouse bound-

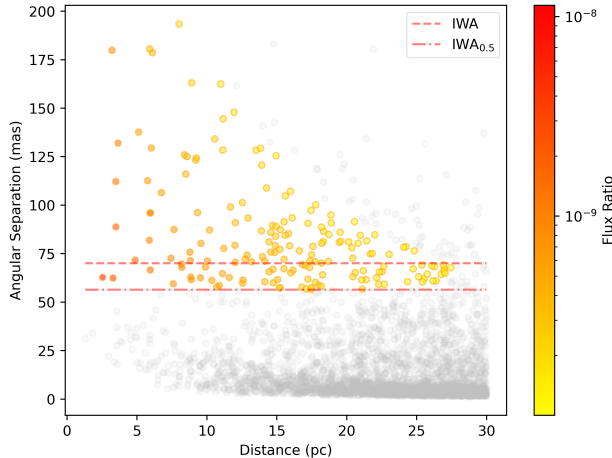


Figure 7. Maximum angular separation of fictitious VZ planets orbiting at the runaway greenhouse boundary around nearby stars with $2500 \text{ K} \leq T_{\text{eff}} \leq 7500 \text{ K}$ within 30 pc. Face-on inclination was assumed and only planets that orbit outside the IWA/IWA_{0.5} while having flux ratios above the 1×10^{-10} threshold are color coded.

aries outward to larger separations and as a result, making planet-star distances larger. Consequently, the planet-to-star flux ratios drop lower because of the large orbital distances. Out of the collected 3814 nearby stars from Gaia, 172 of them may have VZ planets orbiting at the runaway greenhouse boundaries that have large enough angular separations and high enough flux ratios that make them potential future DI targets. Note the face-on inclination Figure 7 assumed means all fictitious VZ planets on circular orbits would have the same phase and angular separation from their host stars throughout their entire orbits. If we were to increase the assumed orbital inclination towards edge-on, VZ planets whose orbits were outside the IWA_{0.5} from the star would have higher maximum flux ratios at smaller phase angles (i.e., smaller angular separation, nearer to the star and the IWA_{0.5} such that a larger fraction of the planetary disk would be illuminated), which would further increase the number of potential VZ planets detectable by future DI missions. However, note that Figure 7 is not a complete representation of the DI detectability for all nearby potential VZ planets thanks to the magnitude limitation of Gaia. Because many bright stars from the Gaia catalog suffer from over-saturation, those with Gaia magnitude $G \leq 7$ were not in the Gaia data (Gaia Collaboration et al. 2016) and thus were not included in the figure.

4.6. Contributions to Future Biosignature Searches and Interpretation

The search for exoplanet biosignatures is one of the fundamental motivating science goals in the design of

future exoplanet observatories (Fujii et al. 2018; Gaudi et al. 2020; The LUVOIR Team 2019). The most referenced biosignature gas is molecule oxygen (O_2), which on Earth is ultimately the result of robust production by photosynthesis organisms (Meadows et al. 2018). In recent years many possible mechanisms for generating abiotic O_2 in planetary atmospheres have been proposed. These abiotic O_2 mechanisms include water loss with the selective retention of O_2 during a runaway greenhouse (e.g. Luger & Barnes 2015; Schaefer et al. 2016; Tian 2015) and the decomposition of CO_2 -rich atmospheres into CO and O_2 in the absence of photochemical catalysts such as HO_x species and/or under the influence of photolysis driven by the UV spectral energy distributions of M dwarf hosts (e.g. Gao et al. 2015; Hu et al. 2020). Importantly, these so-called oxygen false positive mechanisms, while supported by theory, remain speculative—we do not yet have observational evidence of their existence. Venus, for example, contains no free O_2 despite evidence for water loss from the D/H ratio of atmospheric water vapor (Kane et al. 2019). In the case of Venus, O_2 sinks must have outcompeted the net O_2 source from H loss, though this is just one data point. Most of these proposed abiotic O_2 mechanisms would be most efficiently realized for terrestrial planets that orbit in the VZ, where insolation and presumably water loss is more efficient than for planets in the traditional HZ (Luger & Barnes 2015). The VZ then provides a novel opportunity to advance the search for exoplanet biosignatures by testing for the existence of some of the most probable false positives on planets that are the least likely to be inhabited. If O_2 is not found on VZ planets, it may be a more compelling biosignature on HZ worlds. In contrast, if O_2 is common on VZ worlds, we must be more circumspect with biosignature interpretations on planets in the HZ. Abundant abiotic O_2 on VZ planets could be detected via O_2 - O_2 collisionally-induced absorption features at 1.06 and 1.27 μm in transmission spectroscopy and these and additional visible absorption features in reflected light observations (Lincowski et al. 2018; Schwertner et al. 2016, 2018). The best candidates to be observed in search for O_2 signatures are those closest to the outer VZ boundary since they are less likely to have experienced hydrodynamic loss of oxygen in their atmospheres.

5. CONCLUSIONS

In this work we presented a broad overview of the known terrestrial planets in the VZ and provided both measured and estimated data for each. There are currently 317 known terrestrial planets in the VZ, and TESS will continue to provide additional VZ planet can-

dicates as its second extended mission is planned to end in 2025. At the time of writing, the VZ is most heavily populated towards the inner VZ boundary. Although these planets would, in theory, be more amenable to atmospheric observations, their high equilibrium temperature and incident flux make them less useful for comparison to Venus and more susceptible to atmospheric loss. Observations of the atmospheres of VZ planets near the outer VZ boundary present an opportunity to simultaneously study planets which may help understand Venus' past, and test the location of the outer VZ and inner HZ boundaries.

We listed the eight terrestrial VZ planets which are planned to be observed by JWST, including two pairs of neighboring planets from the TRAPPIST-1 and TOI-776 systems. Observations of multiple VZ planets in the same system can give insight into how differences in planet size, planet mass, and incident flux can result in differences in climate over time without needing to factor in the effects of different host stars. The other JWST VZ targets have unique properties, but all can provide valuable information for understanding the different evolutionary pathways of VZ planets. However, the ability of JWST to obtain information about the atmospheres of VZ planets will be highly dependent on their atmospheric composition and cloud coverage, as a Venus-like atmosphere is likely to prevent the detection of any molecular absorption with the time allotted for each planet. However, even a non-detection of molecules in any of the VZ target atmospheres is still valuable since it will illustrate the sensitivity of the JWST instruments and inform future target selection of VZ planets.

Aside from the JWST VZ targets, we chose an additional six terrestrial VZ planets to be considered for future JWST observations. The planets were chosen based on their TSM value, location in the VZ, and size. LTT 1445 A c and L 98-59 d were chosen since studying observations of their atmospheres will be particularly valuable for comparison to their neighboring VZ planets, which are already planned to be observed by

JWST. In general, observations of the five suggested planets can be used to investigate how the onset of a runaway greenhouse, or location of the outer VZ boundary, may be dependent on planet mass, incident flux, and orbital eccentricity. In response to the development of the mission concept, MIRECLE, that can study the atmospheres of non-transiting exoplanets, we also provided six non-transiting VZ planets that cannot be probed by JWST. In comparison to the five transiting targets, almost all of the non-transiting targets are more similar to Venus in size and are located closer to the outer VZ boundary. Their locations make them prime targets for testing the outer VZ boundary, and the previously mentioned mission concept would provide the means to make these planets accessible.

The study of Venus-like exoplanets has become increasingly important given the announcement of several future in-situ Venus missions like DAVINCI+ (Garvin et al. 2022), VERITAS (Cascioli et al. 2021), Venera-D (Zasova et al. 2019; Vorontsov et al. 2011), and EnVision (Widemann et al. 2020). The data gathered from these missions will provide invaluable information about Venus, such as updates on the structure and composition of its atmosphere, determining its water loss history, and compiling a high resolution map of its surface. These missions will inherently benefit exoplanetary science since their data will be used to improve climate models capable of simulating Venus-like surface conditions, which will enhance our ability to predict the climates of VZ planets. Modeling the climates of an assortment of VZ planets will strengthen our understanding of what forced Venus into a runaway greenhouse, test the location of the VZ boundaries, and potentially justify the possibility of a temperate period in Venus' past. In particular if many planets in the VZ are found to have Earth-like surface conditions, it will illustrate that the differences in insolation flux between Earth and Venus is not the primary reason for the divergence between the two planets. All of these results would benefit the study of planetary habitability and help identify future targets for the search for life in the universe.

Table 1. Venus Zone Planet Properties.

Planet	CHZ (%)	VZ (%)	Loc	R_p	$^*(R_\oplus)$	M_p	$^*(M_\oplus)$	P (days)	e	**	a (AU)	T_{eq} (K)	TSM	K (m/s)
Kepler-367 c	0	100	0.437	1.20	1.75	53.58	0	0.253	375	0.83	-			
Kepler-243 c	0	100	0.008	1.99	4.84	20.03	0	0.142	613	3.38	-			
Kepler-261 c	0	100	0.068	1.99	4.94	24.57	0	0.156	553	6.73	-			
Kepler-327 d	0	100	0.270	1.72	4.10	13.97	0	0.090	427	7.75	-			

Table 1 *continued*

Table 1 (*continued*)

Planet	CHZ (%)	VZ (%)	Loc	R_p (* (R_{\oplus}))	M_p (* (M_{\oplus}))	P (days)	e (**)	a (AU)	T_{eq} (K)	TSM	K (m/s)
Kepler-1651 b	0	100	0.180	1.84	4.45	9.88	0.13	0.072	471	24.50	2.070
Kepler-37 c	0	100	0.008	0.75	0.35	21.30	0	0.140	613	5.00	0.095
Proxima Cen b	75	25	-1	1.08	1.27	11.19	0.35	0.049	251	190.71	1.591
TRAPPIST-1 c	0	100	0.557	1.10	1.31	2.42	0	0.016	340	24.27	3.106
LHS 1140 c	0	100	0.332	1.16	1.76	3.78	0.27	0.027	402	32.77	2.272
Kepler-138 b	0	100	0.142	0.64	0.07	10.31	0.02	0.075	494	9.57	0.031
Kepler-138 c	0	100	0.224	1.51	2.30	13.78	0.02	0.091	448	23.25	0.927
Kepler-138 d	0	100	0.415	1.51	2.10	23.09	0.01	0.129	377	21.43	0.713
Kepler-138 e	0	100	0.677	0.79	0.43	38.23	0.11	0.180	319	1.91	0.124
Kepler-49 e	0	100	0.222	1.56	3.55	18.60	0	0.116	450	4.45	-
G 264-012 b	0	100	0.025	1.36	2.50	2.31	0	0.023	593	21.39	2.706
G 264-012 c	0	100	0.368	1.76	3.75	8.05	0	0.053	391	134.07	2.673
GJ 393 b	0	100	0.155	1.19	1.71	7.03	0	0.054	485	28.72	1.004
HD 23472 b	0	100	0.048	1.99	8.32	17.67	0.07	0.116	570	34.54	2.675
HD 23472 c	0	100	0.171	1.87	3.41	29.80	0.06	0.165	479	59.85	0.921
Kepler-52 c	0	100	0.239	1.84	4.36	16.39	0	0.103	442	6.85	1.656
Kepler-171 d	0	100	0.103	1.89	4.64	39.60	0	0.223	528	2.64	-
Kepler-215 e	0	100	0.145	1.75	4.18	68.16	0	0.314	501	2.49	-
YZ Cet c	0	100	0.310	1.04	1.14	3.06	0.00	0.022	410	-	1.858
Kepler-54 c	0	100	0.240	1.23	1.83	12.07	0	0.082	440	0.68	0.797
Kepler-54 d	0	100	0.271	1.52	3.40	21.00	0	0.126	428	3.69	-
Kepler-196 b	0	100	0.031	1.90	4.55	20.74	0	0.138	588	5.20	-
Kepler-1938 b	0	100	0.040	1.83	4.45	13.06	0	0.094	578	5.18	1.611
K2-315 b	0	100	0.195	0.95	0.83	3.14	0	0.023	462	6.66	1.180
LHS 1678 c	0	100	0.090	0.99	0.94	3.69	0.22	0.033	531	14.82	0.812
K2-136 d	0	100	0.222	1.44	2.94	25.58	0.14	0.154	451	2.53	0.788
LP 890-9 b	0	100	0.348	1.32	2.29	2.73	0	0.019	396	10.46	4.324
Kepler-1965 b	0	100	0.090	1.36	2.60	41.87	0	0.230	539	0.43	0.502
K2-400 b	0	100	0.045	1.16	1.65	3.87	0	0.035	572	4.04	1.301
HD 219134 d	0	100	0.323	1.61	16.18	46.86	0.14	0.237	410	35.30	3.334
HD 219134 f	0	100	0.105	1.31	7.30	22.72	0.15	0.146	522	8.05	1.918
TOI-700 d	63	37	-1.000	1.14	1.51	37.42	0.11	0.163	269	3.64	0.527
Kepler-102 f	0	100	0.138	0.88	0.65	27.45	0	0.165	500	1.87	0.159
GJ 357 c	0	100	0.339	1.64	3.40	9.12	0	0.061	401	194.50	2.112
L 98-59 b	0	63	0.008	0.85	0.40	2.25	0.10	0.022	613	52.80	0.468
LP 791-18 b	0	100	0.019	1.12	1.48	0.95	0.00	0.010	599	19.74	3.602
K2-3 c	0	100	0.420	1.28	2.14	24.65	0.00	0.140	376	2.95	0.661
TOI-270 b	0	100	0.035	1.21	1.58	3.36	0.03	0.032	581	12.97	1.266
Kepler-1735 b	0	100	0.070	1.20	1.75	7.72	0	0.062	549	0.97	0.854
GJ 1132 c	0	100	0.620	1.38	2.64	8.93	0.27	0.048	328	18.31	2.651
LT T 1445 A c	0	100	0.113	1.14	1.54	3.12	0.22	0.027	513	44.52	1.701
Kepler-1697 b	0	100	0.203	1.25	1.94	33.50	0	0.185	462	0.67	0.467
Kepler-1948 b	0	100	0.246	1.03	1.09	15.57	0	0.102	438	1.22	0.400
Kepler-1928 b	0	69	0.021	1.99	5.15	19.58	0.43	0.194	600	7.03	1.152
TOI-1266 c	0	100	0.537	1.56	2.20	18.80	0.04	0.106	346	48.25	0.902
TOI-1452 b	0	100	0.630	1.67	4.82	11.06	0.00	0.061	326	38.23	3.493
GJ 1132 b	0	77	0.037	1.13	1.66	1.63	0.22	0.015	579	28.15	2.899
TRAPPIST-1 b	0	100	0.343	1.12	1.37	1.51	0	0.012	398	28.77	3.811
L 98-59 c	0	100	0.103	1.39	2.22	3.69	0.10	0.030	521	36.51	2.202
L 98-59 e	0	100	0.568	1.54	3.06	12.80	0.13	0.072	339	149.23	1.984
LHS 1478 b	0	100	0.022	1.24	2.33	1.95	0	0.018	596	17.81	3.129
TRAPPIST-1 d	0	100	0.881	0.78	0.39	4.05	0	0.022	286	25.16	0.775
YZ Cet b	0	100	0.177	0.91	0.70	2.02	0.06	0.016	472	-	1.310
HD 20794 c	0	100	0.022	1.36	2.42	40.11	0.00	0.204	598	21.44	0.572

Table 1 *continued*

Table 1 (*continued*)

Planet	CHZ (%)	VZ (%)	Loc	R_p	* (R_{\oplus})	M_p	* (M_{\oplus})	P (days)	e	**	a (AU)	T_{eq} (K)	TSM	K (m/s)
Kepler-88 b	0	100	0.209	1.76	4.18		70.70	0	0.331		467	3.91	0.660	
Kepler-445 b	0	100	0.197	1.57	3.47		2.98	0.00	0.023		461	28.62	4.837	
Kepler-446 c	0	100	0.126	1.12	1.39		3.04	0.00	0.025		504	3.21	1.689	
Kepler-1232 b	0	100	0.017	1.93	4.74		26.78	0	0.170		603	2.95	1.071	
Kepler-974 b	0	100	0.001	1.57	3.55		4.19	0	0.041		621	13.87	2.173	
Kepler-1605 b	0	100	0.422	1.08	1.28		85.76	0	0.362		383	0.64	0.206	
Kepler-1608 b	0	100	0.018	1.72	4.14		16.47	0	0.115		602	2.37	1.261	
Kepler-1389 b	0	100	0.614	1.77	4.10		99.25	0	0.391		337	2.35	0.651	
Kepler-1492 b	0	100	0.056	1.49	3.20		16.75	0	0.117		563	0.59	0.950	
Kepler-1439 b	0	100	0.202	1.46	3.00		8.07	0	0.061		459	0.93	1.606	
Kepler-1457 b	0	100	0.080	1.99	5.04		51.11	0	0.270		547	2.73	0.863	
Kepler-1512 b	0	100	0.174	1.18	1.65		20.36	0	0.131		476	1.09	0.475	
Wolf 1061 c	0	100	0.813	1.62	3.41		17.87	0.11	0.089		297	313.54	1.911	
GJ 273 c	0	100	0.226	1.06	1.18		4.72	0.17	0.036		447	72.57	1.041	
GJ 3293 e	0	100	0.423	1.58	3.28		13.25	0.21	0.082		374	75.91	1.616	
Teegarden's Star b	0	100	0.870	1.02	1.05		4.91	0.00	0.025		288	96.05	1.970	
YZ Cet d	0	100	0.487	1.03	1.09		4.66	0.07	0.029		357	-	1.547	
GJ 1061 b	0	100	0.368	1.10	1.37		3.20	0.31	0.021		390	89.07	2.568	
K2-47 b	0	100	0.134	1.89	4.84		31.64	0	0.178		504	5.35	1.185	
K2-72 c	0	100	0.595	1.15	1.60		15.19	0.11	0.078		333	2.58	0.989	
Kepler-55 f	0	100	0.018	1.59	3.55		10.20	0	0.081		601	3.59	-	
GJ 357 b	0	100	0.093	1.22	1.84		3.93	0	0.035		529	29.07	1.509	
K2-316 c	0	100	0.278	1.83	4.55		5.26	0	0.058		423	14.13	2.633	
TOI-237 b	0	100	0.396	1.43	2.82		5.44	0.00	0.034		382	7.83	3.221	
HD 260655 c	0	100	0.059	1.53	3.09		5.71	0.04	0.047		558	196.05	1.913	
K2-129 b	0	100	0.289	1.04	1.13		8.24	0.13	0.057		419	7.05	0.713	
LT T 1445 A b	0	100	0.265	1.30	2.87		5.36	0.11	0.038		429	29.35	2.594	
K2-58 d	0	100	0.001	1.71	4.01		22.88	0	0.152		621	9.33	0.977	
Kepler-37 d	0	100	0.146	1.94	4.64		39.79	0	0.212		498	35.37	1.009	
TOI-2285 b	12	88	0.723	1.74	4.18		27.27	0.30	0.136		311	22.55	1.584	
K2-83 c	0	100	0.206	1.48	3.23		10.00	0	0.071		458	2.36	1.561	
GJ 15 A b	0	100	0.340	1.52	3.03		11.44	0.09	0.072		400	362.38	1.645	
Kepler-52 d	0	100	0.483	1.95	4.79		36.45	0	0.182		361	5.24	-	
K2-285 e	0	100	0.136	1.95	4.84		14.76	0.00	0.180		502	12.42	1.118	
Kepler-137 c	0	100	0.002	1.88	4.55		18.74	0	0.130		620	8.37	-	
Kepler-333 b	0	100	0.124	1.32	2.29		12.55	0	0.087		507	0.93	-	
Kepler-205 c	0	100	0.240	1.64	3.70		20.31	0	0.122		442	10.40	-	
Kepler-388 c	0	100	0.074	0.86	0.58		13.30	0	0.093		546	0.73	-	
Kepler-158 c	0	100	0.245	1.90	4.64		28.55	0	0.158		442	6.14	-	
K2-153 b	0	100	0.074	1.99	4.84		7.52	0	0.061		545	14.38	2.355	
K2-408 b	0	100	0.011	1.68	4.01		20.98	0	0.139		610	12.26	1.071	
K2-318 b	0	100	0.208	1.66	3.93		7.01	0	0.091		456	8.59	1.557	
Kepler-1805 b	0	100	0.100	1.55	3.40		8.85	0	0.070		523	6.96	1.512	
Kepler-1795 b	0	100	0.051	1.66	3.89		13.36	0	0.101		567	3.06	1.248	
Kepler-1846 b	0	100	0.018	1.76	4.18		14.82	0	0.109		602	5.70	1.275	
Kepler-1853 b	0	100	0.295	1.51	3.33		48.89	0	0.240		422	1.84	0.693	
KOI-1831 d	0	100	0.118	1.13	2.23		34.17	0	0.199		515	0.24	0.472	
Kepler-1923 b	0	100	0.017	1.96	4.79		52.61	0	0.284		604	1.80	0.762	
Kepler-1841 b	0	100	0.026	1.49	3.20		25.89	0	0.160		593	0.32	0.788	
GJ 411 b	0	100	0.377	1.40	2.69		12.94	0.06	0.079		389	76.02	1.375	
Kepler-1904 b	0	100	0.001	1.39	2.68		4.58	0	0.044		621	0.93	1.575	
Kepler-1702 b	0	100	0.038	1.60	3.70		18.50	0	0.130		581	2.00	0.995	
GJ 887 b	0	100	0.185	1.90	4.20		9.26	0.00	0.068		468	-	2.058	
K2-184 b	0	100	0.093	1.47	3.07		16.98	0	0.169		534	3.05	0.729	

Table 1 *continued*

Table 1 (*continued*)

Planet	CHZ (%)	VZ (%)	Loc	R_p * (R_{\oplus})	M_p * (M_{\oplus})	P (days)	e **	a (AU)	T_{eq} (K)	TSM	K (m/s)
Kepler-224 e	0	100	0.053	1.97	4.74	18.64	0	0.124	567	3.59	-
Kepler-1749 b	0	100	0.205	1.61	3.85	14.53	0	0.095	458	6.09	1.503
Kepler-1802 b	0	100	0.127	1.67	3.89	15.45	0	0.105	505	3.33	1.331
K2-384 c	0	100	0.066	1.19	1.72	4.19	0	0.035	551	3.14	1.424
K2-384 d	0	100	0.178	1.39	2.60	6.68	0	0.048	472	2.85	1.846
K2-384 e	0	100	0.296	1.34	2.39	9.72	0	0.062	417	2.47	1.500
Ross 508 b	43	57	0.827	1.79	4.00	10.77	0.33	0.054	294	181.81	3.858
Kepler-1816 b	0	100	0.604	1.97	4.94	91.50	0	0.367	339	3.23	0.820
Kepler-225 c	0	100	0.443	1.84	4.45	18.79	0	0.111	369	4.39	-
Kepler-295 d	0	100	0.035	1.36	2.49	33.88	0	0.192	585	0.32	-
K2-5 b	0	100	0.002	1.90	4.55	5.74	0	0.053	620	10.77	2.257
Kepler-353 b	0	100	0.028	0.88	0.65	5.80	0	0.051	589	0.91	-
Kepler-1596 b	0	100	0.200	1.90	4.64	66.37	0	0.315	470	1.47	0.759
HD 39194 d	0	96	0.123	1.81	4.00	33.91	0.33	0.185	512	84.36	1.078
K2-240 c	0	100	0.365	1.80	4.27	20.52	0	0.116	392	19.24	1.474
K2-377 b	0	100	0.091	1.69	3.93	12.83	0	0.100	531	7.76	1.226
K2-381 d	0	100	0.234	1.69	3.77	26.80	0	0.159	446	9.96	0.976
K2-101 b	0	100	0.004	1.99	5.04	14.68	0	0.112	618	12.40	1.486
K2-149 b	0	100	0.210	1.64	3.70	11.33	0	0.083	455	10.69	1.493
Kepler-174 c	0	100	0.356	1.49	3.13	44.00	0	0.214	401	0.58	-
Kepler-225 b	0	100	0.105	1.20	1.72	6.74	0	0.056	520	0.67	-
Kepler-130 d	0	100	0.163	1.64	3.93	87.52	0	0.377	491	3.71	-
Kepler-403 c	0	100	0.001	1.75	4.18	54.28	0	0.297	621	2.43	-
Kepler-186 d	0	100	0.222	1.40	2.71	13.34	0	0.078	449	1.25	1.251
Kepler-42 b	0	100	0.044	0.78	0.42	1.21	0	0.012	572	14.41	0.964
Kepler-1456 b	0	100	0.183	1.14	1.55	18.14	0	0.116	471	0.45	0.507
Kepler-1620 b	0	100	0.165	1.61	3.70	101.95	0	0.447	492	1.43	0.461
Kepler-331 c	0	100	0.218	1.84	4.27	17.28	0	0.105	453	5.26	-
Kepler-386 c	0	100	0.064	1.58	3.62	25.19	0	0.155	557	1.88	-
K2-349 b	0	100	0.055	1.38	2.54	9.03	0	0.069	563	1.19	1.178
Kepler-231 b	0	100	0.186	1.72	4.10	10.07	0	0.074	467	6.40	-
Kepler-1459 b	0	100	0.439	1.36	2.39	62.87	0	0.285	375	0.34	0.454
Kepler-354 c	0	100	0.081	1.31	2.25	16.93	0	0.115	541	0.39	-
Kepler-249 c	0	100	0.140	1.51	3.26	7.11	0	0.058	495	7.77	-
Kepler-329 b	0	100	0.019	1.40	2.71	7.42	0	0.061	599	0.85	-
Kepler-1418 b	0	100	0.113	1.66	3.93	22.48	0	0.143	516	3.03	1.060
K2-133 e	0	100	0.646	1.72	4.10	26.58	0	0.135	324	13.39	1.473
Kepler-383 c	0	100	0.231	1.24	1.90	31.20	0	0.172	448	0.41	-
Kepler-327 c	0	100	0.026	1.03	1.11	5.21	0	0.047	591	1.27	-
Kepler-1505 b	0	100	0.034	0.93	0.75	30.86	0	0.188	587	0.70	0.160
GJ 1061 d	78	22	-1	1.17	1.64	13.03	0.53	0.054	243	54.85	2.149
Kepler-1089 b	0	100	0.032	1.83	4.45	5.13	0	0.047	585	9.38	2.553
Kepler-409 b	0	100	0.263	1.19	1.68	68.96	0	0.320	439	2.40	0.277
Kepler-383 b	0	100	0.016	1.32	2.34	12.90	0	0.095	603	0.53	-
Kepler-231 c	0	100	0.417	1.93	4.74	19.27	0	0.114	377	6.21	-
GJ 581 e	0	100	0.056	1.16	1.68	3.15	0.00	0.028	561	41.80	1.613
CD Cet b	0	100	0.169	1.79	3.95	2.29	0	0.019	476	512.81	6.496
Kepler-430 c	0	100	0.145	1.79	4.36	110.98	0	0.476	502	0.97	0.523
Kepler-1223 b	0	100	0.024	1.22	1.79	16.30	0	0.117	595	0.50	0.523
Kepler-1280 b	0	100	0.031	1.87	4.50	66.56	0	0.342	590	1.58	0.629
Kepler-1441 b	0	100	0.033	1.31	2.25	39.44	0	0.227	588	0.27	0.422
Kepler-167 d	0	100	0.077	1.23	1.86	21.80	0.00	0.140	545	0.59	0.504
GJ 3323 b	0	100	0.514	1.25	2.02	5.36	0.23	0.033	350	133.76	2.564
GJ 625 b	0	100	0.590	1.44	2.82	14.63	0.13	0.078	334	33.59	1.659

Table 1 *continued*

Table 1 (*continued*)

Planet	CHZ (%)	VZ (%)	Loc	R_p (* (R_{\oplus}))	M_p (* (M_{\oplus}))	P (days)	e **	a (AU)	T_{eq} (K)	TSM	K (m/s)
Ross 128 b	0	100	0.743	1.11	1.40	9.87	0.12	0.050	307	70.71	1.372
GJ 3138 c	0	100	0.083	1.88	4.18	5.97	0.11	0.057	537	-	1.911
GJ 1061 c	27	73	0.771	1.18	1.74	6.69	0.29	0.035	302	66.44	2.508
Wolf 1061 b	0	100	0.204	1.22	1.91	4.89	0.15	0.038	457	56.04	1.657
HD 85512 b	0	100	0.562	1.57	3.18	58.43	0.11	0.260	343	84.52	0.856
GJ 251 b	0	100	0.513	1.81	4.00	14.24	0.10	0.082	351	304.90	2.097
HD 215152 e	0	100	0.112	1.49	2.88	25.20	0.00	0.154	518	11.29	0.747
GJ 273 b	29	71	0.921	1.47	2.89	18.65	0.10	0.091	283	50.86	1.598
Kepler-1454 b	0	100	0.158	1.88	4.64	47.03	0	0.246	491	2.26	0.882
Kepler-1599 b	0	100	0.382	1.62	3.66	122.36	0	0.481	399	1.08	0.474
Kepler-438 b	0	100	0.711	1.12	1.45	35.23	0.03	0.166	313	0.80	0.434
K2-72 d	0	100	0.296	1.01	1.04	7.76	0.11	0.050	416	3.28	0.808
Kepler-1570 b	0	100	0.008	1.06	1.23	26.55	0	0.169	613	0.46	0.279
K2-21 b	0	85	0.023	1.84	4.41	9.33	0.10	0.076	595	22.24	1.743
K2-72 e	20	81	0.894	1.29	2.11	24.16	0.11	0.106	286	2.32	1.123
K2-88 b	0	100	0.184	1.23	1.94	4.61	0	0.035	468	4.96	1.834
K2-13 b	0	100	0.104	1.89	4.74	39.91	0	0.211	528	7.34	1.031
K2-50 b	0	100	0.035	1.59	3.47	8.75	0	0.071	583	9.27	1.498
K2-54 b	0	100	0.251	1.15	1.58	9.78	0	0.067	436	2.38	0.841
EPIC 211822797 b	0	100	0.263	1.92	4.74	21.17	0	0.120	431	8.38	1.557
K2-72 b	0	100	0.189	1.08	1.28	5.58	0.11	0.040	465	3.62	1.111
Kepler-296 c	0	82	0.071	1.99	4.94	5.84	0.33	0.052	547	10.07	2.900
Kepler-202 c	0	100	0.072	1.85	4.45	16.28	0	0.113	548	7.72	-
Kepler-298 b	0	100	0.038	1.96	4.74	10.48	0	0.080	580	6.22	-
Kepler-286 e	0	100	0.025	1.77	4.18	29.22	0	0.176	595	1.78	-
Kepler-186 c	0	100	0.027	1.25	1.94	7.27	0	0.045	591	1.65	1.181
Kepler-316 c	0	100	0.013	1.15	1.51	6.83	0	0.058	607	0.94	-
Kepler-331 b	0	100	0.042	1.81	4.36	8.46	0	0.065	576	6.31	-
Kepler-329 c	0	100	0.244	1.93	4.74	18.68	0	0.113	440	6.14	-
Kepler-801 b	0	100	0.041	1.99	4.99	11.42	0	0.087	576	5.82	1.851
Kepler-1397 b	0	100	0.022	1.71	4.18	47.45	0	0.264	599	1.95	0.698
Kepler-80 g	0	100	0.076	1.13	1.51	14.65	0	0.110	544	0.42	0.448
Kepler-1391 b	0	100	0.070	1.68	3.81	54.41	0	0.284	554	2.05	0.631
Kepler-353 c	0	100	0.102	1.38	2.65	8.41	0	0.065	522	0.74	-
Kepler-779 b	0	100	0.111	0.92	0.75	7.10	0	0.056	515	1.07	0.418
Kepler-367 b	0	100	0.296	1.30	2.20	37.82	0	0.201	421	0.94	-
Kepler-296 b	0	100	0.231	1.61	3.77	10.86	0.33	0.079	445	5.67	1.798
K2-155 d	0	100	0.505	1.90	4.64	40.72	0	0.194	355	18.70	1.170
Kepler-973 b	0	100	0.250	1.96	4.84	49.61	0	0.251	443	6.10	0.931
Kepler-504 b	0	100	0.355	1.59	3.62	9.55	0	0.061	395	20.23	2.284
Kepler-62 e	0	100	0.920	1.61	3.70	122.39	0	0.427	289	3.34	0.609
Kepler-62 d	0	100	0.078	1.95	4.74	18.16	0	0.120	544	8.67	1.473
Kepler-260 c	0	100	0.343	1.74	4.01	76.05	0	0.332	407	2.38	-
Kepler-332 c	0	100	0.019	1.09	1.31	16.00	0	0.114	600	0.66	-
Kepler-446 d	0	100	0.279	1.34	2.44	5.15	0.00	0.035	423	2.65	2.479
Kepler-1498 b	0	100	0.214	1.33	2.34	48.05	0	0.246	460	0.24	0.455
Kepler-174 b	0	100	0.033	1.96	4.94	13.98	0	0.100	586	8.10	-
Kepler-878 b	0	100	0.091	1.93	4.74	25.94	0	0.160	534	3.64	1.178
K2-239 c	0	100	0.305	1.00	0.98	7.78	0	0.058	413	4.42	0.577
Kepler-236 c	0	100	0.498	1.99	5.15	23.97	0	0.132	355	6.00	-
Kepler-560 b	0	100	0.674	1.71	4.01	18.48	0	0.095	319	16.21	1.993
Kepler-125 c	0	100	0.036	0.74	0.34	5.77	0	0.051	581	1.60	-
Kepler-345 c	0	100	0.005	1.20	1.75	9.39	0	0.077	616	1.03	-
Kepler-299 e	0	100	0.034	1.87	4.64	38.29	0	0.220	586	1.65	-

Table 1 *continued*

Table 1 (*continued*)

Planet	CHZ (%)	VZ (%)	Loc	R_p *(R_{\oplus})	M_p *(M_{\oplus})	P (days)	e	**	a (AU)	T_{eq} (K)	TSM	K (m/s)
K2-239 b	0	100	0.178	1.10	1.37	5.24	0	0.044	472	4.97	0.919	
Kepler-384 c	0	100	0.115	1.13	1.48	45.35	0	0.236	519	0.41	-	
Kepler-220 d	0	100	0.221	0.97	0.90	28.12	0	0.163	453	1.13	-	
Kepler-1124 b	0	100	0.004	1.28	2.09	2.85	0	0.028	618	1.86	1.896	
K2-148 d	0	100	0.053	1.64	3.70	9.76	0	0.077	564	12.88	1.473	
Kepler-399 d	0	100	0.291	1.89	4.74	58.03	0	0.261	428	3.87	-	
Kepler-445 d	0	100	0.611	1.23	1.86	8.15	0.00	0.045	330	2.79	1.857	
Kepler-132 e	0	100	0.244	1.18	1.65	110.29	0	0.455	452	0.49	0.215	
Kepler-249 d	0	100	0.395	1.57	3.51	15.37	0	0.097	383	6.23	-	
Kepler-1251 b	0	100	0.123	1.84	4.36	45.09	0	0.241	514	2.09	0.828	
Kepler-1480 b	0	100	0.034	1.67	3.93	22.13	0	0.146	585	3.22	0.998	
Kepler-149 c	0	100	0.182	1.61	3.70	55.33	0	0.281	477	2.19	-	
Kepler-399 c	0	100	0.067	1.43	2.79	26.68	0	0.155	556	0.56	-	
Kepler-1006 b	0	100	0.012	1.53	3.40	19.76	0	0.132	609	3.65	0.949	
Kepler-186 e	0	100	0.411	1.27	2.07	22.41	0	0.110	378	1.02	0.805	
Kepler-395 b	0	100	0.000	1.03	1.11	7.05	0	0.061	623	0.64	-	
Kepler-236 b	0	100	0.123	1.57	3.40	8.30	0	0.065	507	6.30	-	
Kepler-220 e	0	100	0.402	1.33	2.39	45.90	0	0.226	385	0.93	-	
Kepler-378 b	0	100	0.070	0.75	0.35	16.09	0	0.112	550	1.88	-	
Kepler-81 d	0	100	0.194	1.21	1.75	20.84	0	0.128	466	0.60	-	
K2-354 b	0	100	0.021	1.56	3.55	3.79	0	0.036	598	19.12	2.551	
Kepler-235 c	0	100	0.022	1.28	2.11	7.82	0	0.065	597	0.60	-	
Kepler-85 e	0	100	0.009	1.27	2.02	25.22	0	0.163	613	0.29	-	
Kepler-332 d	0	100	0.197	1.18	1.68	34.21	0	0.189	466	0.51	-	
Kepler-1126 b	0	100	0.350	1.72	4.06	108.59	0	0.433	410	1.93	0.575	
Kepler-378 c	0	100	0.224	0.69	0.27	28.91	0	0.166	452	1.60	-	
Kepler-398 c	0	100	0.044	1.01	1.02	11.42	0	0.087	574	1.46	-	
Kepler-916 b	0	100	0.104	1.76	4.36	32.30	0	0.188	525	2.15	0.976	
Kepler-303 c	0	100	0.066	1.14	1.55	7.06	0	0.057	552	1.45	-	
Kepler-362 c	0	100	0.115	1.44	2.88	37.87	0	0.207	521	0.43	-	
Kepler-369 c	0	100	0.380	1.41	2.79	14.87	0	0.094	387	0.75	-	
Kepler-395 c	0	100	0.464	1.32	2.32	34.99	0	0.177	366	0.38	-	
Kepler-298 c	0	100	0.236	1.93	4.64	22.93	0	0.136	445	4.63	-	
Kepler-1460 b	0	100	0.278	1.96	4.84	29.96	0	0.168	426	2.83	1.263	
Kepler-333 c	0	100	0.327	1.11	1.39	24.09	0	0.135	407	0.72	-	
Kepler-1410 b	0	100	0.802	1.78	4.10	60.87	0	0.260	300	2.77	0.907	
Kepler-120 c	0	100	0.158	1.52	3.33	12.79	0	0.088	485	5.74	-	
Kepler-371 b	0	100	0.013	1.89	4.64	34.76	0	0.200	608	3.29	-	
Kepler-1646 b	0	100	0.227	1.23	1.83	4.49	0	0.033	446	3.42	1.832	
Kepler-195 c	0	100	0.125	1.55	3.40	34.10	0	0.197	511	2.26	-	
Kepler-1423 b	0	100	0.093	1.06	1.26	23.96	0	0.150	532	0.43	0.326	
Kepler-140 c	0	100	0.123	1.80	4.18	91.35	0	0.414	517	2.20	-	
Kepler-42 d	0	100	0.136	0.57	0.13	1.87	0	0.015	497	15.12	0.267	
Kepler-296 e	33	67	0.769	1.52	3.20	34.14	0.33	0.169	304	3.86	1.042	
Kepler-1499 b	0	100	0.225	1.19	1.68	44.20	0	0.229	454	0.56	0.347	
K2-150 b	0	100	0.300	1.99	5.04	10.59	0	0.073	415	16.07	2.467	
Kepler-124 c	0	100	0.012	1.75	4.18	13.82	0	0.100	608	6.63	-	
Kepler-1135 b	0	100	0.248	1.85	4.55	76.96	0	0.349	447	2.06	0.702	
Kepler-1185 b	0	100	0.420	1.33	2.29	104.35	0	0.428	387	0.53	0.320	
Kepler-32 c	0	100	0.208	1.99	4.84	8.75	0	0.090	456	6.34	1.894	
K2-151 b	0	100	0.003	1.49	3.26	3.84	0	0.037	619	3.51	2.204	
Kepler-1178 b	0	100	0.159	1.06	1.26	31.81	0	0.182	488	0.54	0.294	
Kepler-1582 b	0	100	0.233	1.49	3.20	4.84	0	0.037	443	2.13	2.822	
EPIC 201170410.02	0	100	0.135	1.04	1.16	6.80	0.00	0.035	498	2.39	1.028	

Table 1 *continued*

Table 1 (*continued*)

Planet	CHZ (%)	VZ (%)	Loc	R_p	* (R_{\oplus})	M_p	* (M_{\oplus})	P (days)	e	**	a (AU)	T_{eq} (K)	TSM	K (m/s)
Kepler-992 b	0	100	0.061	1.62	<i>3.70</i>	20.16	0	0.135	559	6.22	1.007			
Kepler-62 c	0	100	0.003	0.54	<i>0.11</i>	12.44	0	0.093	619	1.38	0.038			
K2-339 b	0	100	0.065	1.92	<i>4.74</i>	19.51	0	0.128	555	5.05	1.376			
Kepler-1093 c	0	100	0.136	1.96	<i>4.94</i>	89.72	0	0.409	510	1.87	0.650			
TOI-540 b	0	100	0.009	0.91	<i>0.70</i>	1.24	0.00	0.012	611	38.23	1.421			
TOI-776 b	0	100	0.114	1.85	4.00	8.25	0.06	0.065	513	70.42	1.911			
Kepler-1633 b	0	100	0.329	1.58	<i>3.47</i>	186.40	0	0.679	421	1.12	0.344			
Kepler-1489 b	0	100	0.289	1.77	<i>4.18</i>	82.29	0	0.361	430	1.63	0.646			
Kepler-124 d	0	100	0.198	1.11	<i>1.39</i>	30.95	0	0.170	466	0.59	-			
Kepler-1465 b	0	100	0.218	1.77	<i>4.10</i>	31.83	0	0.179	454	4.39	1.002			
Kepler-371 c	0	100	0.170	1.78	<i>4.18</i>	67.97	0	0.313	486	2.43	-			
Kepler-331 d	0	100	0.456	1.64	<i>3.70</i>	32.13	0	0.159	368	3.49	-			
Kepler-1246 b	0	100	0.003	1.36	<i>2.44</i>	11.32	0	0.089	620	0.56	0.857			
Kepler-1253 b	0	100	0.119	1.33	<i>2.39</i>	68.89	0	0.326	519	0.43	0.380			
Kepler-296 f	78	22	-1.000	1.80	<i>4.32</i>	63.34	0.33	0.255	247	3.85	1.146			
Kepler-330 c	0	100	0.007	1.95	<i>4.74</i>	15.96	0	0.116	615	3.94	-			
Kepler-1440 b	0	100	0.057	1.25	<i>1.94</i>	39.86	0	0.227	565	0.30	0.369			
Kepler-737 b	0	100	0.600	1.96	<i>4.94</i>	28.60	0	0.146	333	7.27	1.618			
K2-133 c	0	100	0.046	1.60	<i>3.70</i>	4.87	0	0.043	571	22.93	2.339			
Kepler-69 c	0	100	0.680	1.71	<i>4.01</i>	242.46	0.14	0.640	329	1.62	0.504			
Kepler-341 e	0	100	0.026	1.99	<i>4.94</i>	42.47	0	0.242	595	2.40	-			
Kepler-1384 b	0	100	0.009	1.94	<i>4.64</i>	15.36	0	0.111	612	3.86	1.409			
Kepler-452 b	0	100	0.996	1.62	<i>3.77</i>	384.84	0	1.046	286	1.08	0.324			
Kepler-1177 b	0	100	0.344	1.90	<i>4.74</i>	106.25	0	0.436	411	1.71	0.648			
Kepler-1638 b	0	100	0.860	1.87	<i>4.55</i>	259.34	0	0.788	302	1.18	0.465			
Kepler-1166 b	0	100	0.072	1.69	<i>3.93</i>	33.24	0	0.195	551	2.62	0.839			
Kepler-176 e	0	100	0.218	1.44	<i>2.94</i>	51.17	0	0.257	458	0.31	0.556			
K2-239 d	0	100	0.408	1.10	<i>1.37</i>	10.12	0	0.069	378	3.95	0.738			
Kepler-1353 b	0	100	0.135	1.80	<i>4.55</i>	24.75	0	0.152	502	2.67	1.198			
Kepler-795 b	0	100	0.002	1.68	<i>3.93</i>	29.62	0	0.184	621	3.82	0.847			
Kepler-440 b	40	60	0.802	1.90	<i>4.64</i>	101.11	0.34	0.242	300	4.59	1.189			
Kepler-1450 b	0	100	0.495	1.71	<i>4.10</i>	54.51	0	0.251	359	2.21	0.868			
Kepler-1649 b	0	100	0.564	1.02	<i>1.02</i>	8.69	0	0.048	339	2.41	0.929			
Kepler-1277 b	0	100	0.085	1.60	<i>3.47</i>	40.84	0	0.227	541	2.54	0.672			
Kepler-1470 b	0	100	0.010	1.06	<i>1.23</i>	16.30	0	0.117	610	0.39	0.360			
Kepler-354 d	0	100	0.169	1.24	<i>1.94</i>	24.21	0	0.146	480	0.34	-			
K2-240 b	0	100	0.028	1.99	<i>5.04</i>	6.03	0	0.051	590	33.18	2.615			
K2-336 b	0	100	0.003	1.22	<i>1.83</i>	21.19	0	0.143	620	0.93	0.466			
K2-368 d	0	100	0.132	1.95	<i>4.69</i>	20.20	0	0.132	503	10.92	1.334			
K2-381 c	0	100	0.095	1.99	<i>5.04</i>	16.03	0	0.113	529	14.49	1.549			
L 98-59 d	0	100	0.308	1.52	1.94	7.45	0.07	0.049	412	274.95	1.518			
TOI-700 b	0	100	0.293	1.04	<i>1.16</i>	9.98	0.08	0.068	418	5.60	0.623			
GJ 3929 b	0	100	0.050	1.09	1.75	2.62	0.00	0.025	567	14.08	1.773			

* Values that are italicized in the planet radius (R_p) and mass (M_p) columns indicate that they were determined using a mass-radius relationship rather than being from observations.

**Planets that did not have a measured eccentricity are denoted by an italicized 0.

An extended version of the table is available in electronic version, which provides uncertainties for all relevant parameters.

Table 2. Venus Zone Host Star Properties.

Host Star	R (R_{\odot})	M (M_{\odot})	Teff	logg	L (L_{\odot})	Jmag	Vmag	[Fe/H] (dex)	Dist
CD Cet	0.17	0.16	3130	4.93	0.003	8.775	13.950	0.13	8.61
EPIC 201170410	0.28	0.29	3648	5.00	0.012	13.464	17.698	-0.05	-1.00
EPIC 211822797	0.58	0.62	4057	4.70	0.082	12.277	15.133	0.20	186.20
G 264-012	0.30	0.30	3326	4.85	0.011	8.837	13.078	0.10	16.01
GJ 1061	0.16	0.12	2953	-	0.002	7.523	12.700	-0.08	3.67
GJ 1132	0.21	0.18	3270	-	0.004	9.245	13.680	0.00	12.61
GJ 15 A	0.38	0.38	3607	4.87	0.022	5.252	8.090	-0.34	3.56
GJ 251	0.36	0.36	3451	4.96	0.017	6.104	9.890	-0.03	5.58
GJ 273	0.29	0.29	3382	-	0.009	5.714	9.840	0.09	5.92
GJ 3138	0.50	0.68	3717	-	0.045	-	10.828	-0.30	28.47
GJ 3293	0.40	0.42	3466	-	0.022	8.362	11.945	0.02	20.19
GJ 3323	0.12	0.16	3159	-	0.003	7.617	12.570	-0.27	5.37
GJ 357	0.34	0.34	3505	4.94	0.016	7.337	10.910	-0.12	9.44
GJ 3929	0.32	0.31	3384	4.89	0.011	8.694	12.675	-0.02	15.81
GJ 393	0.43	0.43	3579	4.88	0.027	6.176	9.650	-0.09	7.03
GJ 411	0.37	0.39	3719	4.89	0.024	4.320	7.490	-0.36	5.68
GJ 581	0.33	0.31	3396	4.89	0.013	6.706	10.570	0.00	6.30
GJ 625	0.31	0.30	3499	4.94	0.013	6.608	10.066	-0.38	6.47
GJ 887	0.47	0.49	3688	4.78	0.037	-	-	-0.06	3.29
HD 20794	1.08	0.70	5401	4.22	0.883	3.032	4.260	-0.40	6.00
HD 215152	0.73	0.77	4935	4.40	0.284	6.353	8.110	-0.10	21.60
HD 219134	0.78	0.81	4699	4.57	0.265	3.981	5.569	0.11	6.53
HD 23472	0.71	0.67	4684	4.53	0.237	7.865	9.730	-0.20	39.03
HD 260655	0.44	0.44	3803	5.20	0.036	6.674	9.630	-0.43	10.01
HD 39194	0.74	0.67	5205	4.53	0.390	6.598	8.090	-0.61	26.41
HD 85512	0.71	0.43	4300	4.36	0.155	5.451	7.670	-0.26	11.28
K2-101	0.76	0.82	4927	4.59	0.306	11.162	12.892	0.07	188.33
K2-129	0.36	0.36	3459	-	0.017	9.697	13.639	0.00	27.80
K2-13	0.78	0.80	5698	-	0.576	11.571	12.882	-0.54	342.39
K2-133	0.46	0.46	3655	-	0.033	11.084	14.073	0.00	75.17
K2-136	0.66	0.74	4499	4.66	0.163	9.096	11.101	0.15	59.25
K2-148	0.63	0.65	4079	4.65	0.101	11.082	13.627	-0.11	124.46
K2-149	0.57	0.59	3745	4.71	0.049	11.452	14.543	0.11	123.68
K2-150	0.44	0.46	3499	4.82	0.026	12.107	15.784	0.09	102.48
K2-151	0.45	0.47	3695	4.80	0.034	10.930	14.175	-0.19	69.48
K2-153	0.53	0.55	3845	4.73	0.055	12.023	14.960	-0.09	143.13
K2-155	0.58	0.65	4258	4.60	0.099	10.274	12.773	-0.30	72.80
K2-184	0.75	0.84	5245	4.62	0.382	8.920	10.345	-0.10	75.59
K2-21	0.65	0.68	4222	-	0.121	10.251	12.851	0.00	83.64
K2-239	0.36	0.40	3420	4.90	0.016	10.781	14.632	-0.10	31.08
K2-240	0.54	0.58	3810	4.70	0.053	10.394	13.372	-0.10	72.91
K2-285	0.79	0.83	4975	4.40	0.343	10.477	12.075	0.00	154.96
K2-3	0.56	0.60	3896	4.73	0.065	9.421	12.168	-0.32	44.07
K2-315	0.20	0.17	3300	5.09	0.004	12.665	17.670	-0.24	56.97
K2-316	0.38	0.41	3436	4.89	0.018	12.717	17.140	0.00	112.49
K2-318	0.55	0.56	3851	4.70	0.060	12.042	15.800	0.00	147.87
K2-336	0.80	0.86	5424	4.56	0.498	11.291	12.803	-0.17	239.29
K2-339	0.72	0.74	4857	4.59	0.259	12.796	14.487	-0.11	360.36
K2-349	0.49	0.54	4385	4.78	0.080	12.743	14.585	-0.66	453.57
K2-354	0.41	0.43	3669	4.86	0.027	11.776	15.296	-0.04	91.72
K2-368	0.66	0.75	4663	4.67	0.185	11.613	13.581	-0.25	206.61
K2-377	0.69	0.82	4200	4.67	0.133	11.739	14.107	-0.01	195.15
K2-381	0.68	0.75	4473	4.65	0.166	10.970	12.883	-0.24	145.70

Table 2 *continued*

Table 2 (*continued*)

Host Star	R (R _⊕)	M (M _⊕)	Teff	logg	L (L _⊕)	Jmag	Vmag	[Fe/H] (dex)	Dist
K2-384	0.35	0.33	3623	4.87	0.019	12.118	16.120	0.07	82.66
K2-400	0.38	0.37	3578	4.85	0.021	11.262	15.108	-0.05	62.38
K2-408	0.78	0.81	5335	4.56	0.443	10.427	12.056	-0.17	162.31
K2-47	0.76	0.75	5054	4.54	0.339	12.295	14.065	0.00	349.88
K2-5	0.57	0.61	3930	4.71	0.070	12.449	14.974	-0.33	202.94
K2-50	0.55	0.61	4326	4.74	0.095	12.410	14.705	0.00	257.44
K2-54	0.38	0.42	3798	4.89	0.027	11.850	14.542	0.00	174.96
K2-58	0.86	0.89	5413	4.52	0.570	10.765	12.415	0.00	181.75
K2-72	0.33	0.27	3361	-	0.012	11.685	15.370	0.00	66.43
K2-83	0.42	0.48	3910	4.86	0.037	11.599	14.522	0.00	125.53
K2-88	0.26	0.26	3537	5.02	0.010	12.037	15.523	0.00	110.56
KOI-1831	0.83	0.90	5233	-	0.464	12.783	14.222	0.00	501.57
Kepler-1006	0.74	0.78	5328	4.59	0.396	13.053	14.467	-0.40	-1.00
Kepler-102	0.74	0.80	4903	4.61	0.284	9.984	12.072	0.08	107.80
Kepler-1089	0.49	0.52	3753	4.76	0.043	13.255	16.233	-0.09	259.33
Kepler-1093	1.20	1.13	6166	4.33	1.870	12.807	13.781	-0.01	1072.88
Kepler-1124	0.34	0.35	3658	4.93	0.019	13.671	16.745	-0.59	289.90
Kepler-1126	0.93	0.92	5798	4.46	0.878	12.966	14.221	-0.26	635.74
Kepler-1135	0.94	0.96	5656	4.47	0.812	13.161	14.545	0.02	1314.64
Kepler-1166	0.86	0.90	5446	4.53	0.584	13.223	14.650	-0.02	634.91
Kepler-1177	0.97	0.98	5712	4.46	0.900	13.350	14.773	0.02	1299.97
Kepler-1178	0.75	0.80	4990	4.59	0.313	12.323	14.212	-0.05	482.29
Kepler-1185	0.87	0.96	5622	4.54	0.679	11.386	12.630	-0.04	459.27
Kepler-120	0.53	-	4096	4.73	0.071	13.019	14.995	0.00	388.63
Kepler-1223	0.75	0.80	4870	4.60	0.284	13.055	14.911	0.04	459.96
Kepler-1232	0.89	0.92	5471	4.51	0.638	13.451	14.970	0.06	632.87
Kepler-124	0.64	-	4984	4.67	0.227	12.780	14.400	0.00	420.05
Kepler-1246	0.69	0.73	4611	4.63	0.193	13.286	15.270	-0.03	436.51
Kepler-125	0.51	-	3810	4.74	0.049	12.484	15.431	0.00	183.37
Kepler-1251	0.89	0.92	5545	4.51	0.673	13.724	15.024	-0.04	902.20
Kepler-1253	1.10	0.97	5850	4.33	1.273	11.387	12.588	-0.14	514.52
Kepler-1277	0.92	0.94	5578	4.49	0.736	12.873	14.306	-0.01	557.19
Kepler-1280	1.32	1.20	6227	4.28	2.353	12.966	14.196	0.04	1486.70
Kepler-130	1.13	-	5884	4.30	1.375	10.810	11.572	0.00	316.66
Kepler-132	1.10	1.03	6023	4.37	1.430	10.797	11.922	-0.13	349.55
Kepler-1353	0.72	0.76	4776	4.61	0.242	13.850	15.734	-0.06	593.38
Kepler-137	0.80	-	5187	4.55	0.416	11.650	13.063	0.00	302.98
Kepler-138	0.54	0.54	3841	4.71	0.056	10.293	13.040	-0.18	66.86
Kepler-1384	0.74	0.78	4919	4.60	0.288	13.786	15.758	-0.06	-1.00
Kepler-1389	0.74	0.81	5078	4.61	0.327	13.247	14.896	-0.14	497.09
Kepler-1391	1.10	1.03	5840	4.36	1.264	12.726	13.906	0.04	1038.35
Kepler-1397	1.12	1.09	6026	4.37	1.486	12.849	14.324	0.00	1198.25
Kepler-140	1.29	-	6077	4.27	2.039	11.989	13.018	0.00	583.86
Kepler-1410	0.60	0.63	4092	4.67	0.091	13.586	16.319	0.01	-1.00
Kepler-1418	0.72	0.77	4770	4.61	0.241	13.407	15.461	0.00	-1.00
Kepler-1423	0.75	0.79	4939	4.59	0.301	13.003	14.721	-0.02	-1.00
Kepler-1439	0.43	0.46	3578	4.83	0.027	13.577	17.048	-0.03	225.39
Kepler-1440	0.96	0.98	5698	4.46	0.873	12.951	14.240	0.04	1115.35
Kepler-1441	1.00	1.00	5802	4.45	1.018	13.080	14.290	0.01	1110.48
Kepler-1450	0.68	0.71	4524	4.63	0.174	13.681	15.923	-0.02	505.83
Kepler-1454	0.86	0.90	5448	4.53	0.585	13.623	15.009	-0.02	780.57
Kepler-1456	0.62	0.64	4231	4.67	0.111	13.486	15.777	-0.09	370.31
Kepler-1457	1.01	1.01	5866	4.43	1.085	12.944	14.066	-0.05	889.89
Kepler-1459	0.74	0.78	4828	4.61	0.267	13.005	14.893	0.01	455.48

Table 2 *continued*

Table 2 (*continued*)

Host Star	R (R _☉)	M (M _☉)	Teff	logg	L (L _☉)	Jmag	Vmag	[Fe/H] (dex)	Dist
Kepler-1460	0.67	0.70	4422	4.64	0.154	14.093	16.166	-0.02	553.22
Kepler-1465	0.71	0.75	4726	4.62	0.226	12.718	14.724	-0.06	359.50
Kepler-1470	0.76	0.80	4961	4.59	0.314	13.492	15.252	-0.01	590.60
Kepler-1480	0.81	0.85	5156	4.56	0.417	13.080	14.703	0.07	500.89
Kepler-1489	0.90	0.93	5655	4.51	0.744	13.677	14.983	-0.13	1283.05
Kepler-149	0.95	-	5381	4.46	0.680	12.694	14.152	0.00	571.03
Kepler-1492	0.72	0.77	4712	4.62	0.230	12.804	14.689	0.06	331.55
Kepler-1498	0.81	0.86	5256	4.56	0.450	13.703	15.352	-0.01	-1.00
Kepler-1499	0.78	0.82	5097	4.58	0.369	12.016	13.676	-0.01	309.87
Kepler-1505	0.86	0.93	5686	4.54	0.694	11.830	13.043	-0.18	495.15
Kepler-1512	0.67	0.73	4372	4.64	0.147	11.315	13.451	0.20	-1.00
Kepler-1570	0.89	0.92	5550	4.50	0.675	12.489	14.242	-0.04	919.00
Kepler-158	0.62	-	4623	4.66	0.158	12.722	14.743	0.00	315.18
Kepler-1582	0.30	0.28	3208	4.93	0.009	13.285	17.960	0.48	78.89
Kepler-1596	0.92	0.95	5706	4.49	0.806	14.250	15.632	-0.11	2146.23
Kepler-1599	0.99	0.99	5767	4.45	0.974	13.735	14.970	0.02	1328.20
Kepler-1605	0.82	0.86	5280	4.55	0.469	11.064	12.592	-0.01	546.23
Kepler-1608	0.72	0.75	4992	4.61	0.289	14.419	16.265	-0.24	-1.00
Kepler-1620	1.23	1.15	6157	4.31	1.953	12.559	13.690	0.03	895.07
Kepler-1633	1.32	1.20	6256	4.27	2.398	12.447	13.516	0.02	1114.91
Kepler-1638	0.95	0.97	5710	4.47	0.862	13.550	14.769	-0.01	1525.52
Kepler-1646	0.26	0.24	3299	5.01	0.007	12.872	16.842	0.04	127.59
Kepler-1649	0.23	0.20	3240	5.00	0.005	13.379	17.950	-0.15	92.19
Kepler-1651	0.50	0.52	3713	-	0.043	10.648	13.860	-0.16	66.41
Kepler-167	0.75	0.78	4884	4.58	0.289	12.446	14.284	0.02	341.91
Kepler-1697	0.77	0.75	4682	4.54	0.258	11.760	13.556	0.03	247.77
Kepler-1702	0.73	0.85	5093	4.65	0.319	14.411	16.231	0.00	857.14
Kepler-171	0.84	-	5642	4.57	0.642	13.586	15.101	0.00	863.86
Kepler-1735	0.51	0.54	3975	4.75	0.058	13.035	15.896	-0.34	245.30
Kepler-174	0.62	-	4880	4.68	0.196	12.791	14.530	0.00	384.76
Kepler-1749	0.55	0.55	3957	4.69	0.067	12.663	14.950	-0.16	268.20
Kepler-176	0.83	0.87	5295	4.55	0.486	13.097	14.767	0.03	527.32
Kepler-1795	0.69	0.77	4500	4.64	0.175	13.796	16.188	0.28	-1.00
Kepler-1802	0.64	0.65	4245	4.64	0.119	13.732	15.905	0.00	636.69
Kepler-1805	0.55	0.58	3867	4.72	0.061	12.656	15.536	0.10	221.64
Kepler-1816	0.71	0.79	5051	4.63	0.295	13.042	14.734	-0.24	437.82
Kepler-1841	0.90	0.82	5190	4.45	0.528	13.245	14.855	0.12	631.70
Kepler-1846	0.73	0.79	4825	4.60	0.259	12.554	14.412	0.08	374.62
Kepler-1853	0.79	0.77	4821	4.53	0.303	13.404	15.229	0.16	562.35
Kepler-186	0.47	0.48	3788	4.77	0.041	12.473	15.138	-0.28	177.59
Kepler-1904	0.50	0.53	3805	4.77	0.047	13.523	16.367	-0.10	270.85
Kepler-1923	1.29	1.11	5881	4.26	1.788	13.002	14.454	0.16	990.84
Kepler-1928	0.92	1.01	5720	-	0.809	11.456	12.679	0.12	326.36
Kepler-1938	0.66	0.65	4522	4.62	0.164	13.221	15.246	-0.22	421.15
Kepler-1948	0.56	0.58	3872	4.71	0.063	11.706	14.569	0.12	193.90
Kepler-195	0.78	-	5329	4.60	0.441	13.531	14.863	0.00	652.05
Kepler-196	0.78	-	5128	4.57	0.378	12.752	14.239	0.00	451.31
Kepler-1965	0.84	0.93	5852	4.56	0.743	12.530	13.839	-0.30	521.79
Kepler-202	0.67	-	4668	4.65	0.191	12.255	14.178	0.00	285.11
Kepler-205	0.55	-	4321	4.74	0.095	11.608	13.779	0.00	159.72
Kepler-215	1.03	-	5739	4.36	1.034	12.417	13.678	0.00	486.00
Kepler-220	0.67	-	4632	4.65	0.186	11.206	13.049	0.00	171.11
Kepler-224	0.68	-	5018	4.64	0.263	14.212	15.801	0.00	782.09
Kepler-225	0.48	-	3682	4.78	0.038	14.032	16.294	0.00	561.10

Table 2 *continued*

Table 2 (*continued*)

Host Star	R (R _⊕)	M (M _⊕)	Teff	logg	L (L _⊕)	Jmag	Vmag	[Fe/H] (dex)	Dist
Kepler-231	0.49	-	3767	4.78	0.043	13.405	15.813	0.00	316.62
Kepler-235	0.55	-	4255	4.73	0.089	13.952	16.567	0.00	428.02
Kepler-236	0.51	-	3750	4.75	0.046	13.224	16.014	0.00	288.76
Kepler-243	0.84	-	5228	4.57	0.474	13.622	15.159	0.00	693.86
Kepler-249	0.48	-	3568	4.78	0.034	12.836	16.370	0.00	190.40
Kepler-260	0.86	-	5250	4.49	0.505	12.900	14.253	0.00	627.37
Kepler-261	0.79	-	5098	4.56	0.379	12.127	13.738	0.00	317.50
Kepler-286	0.86	-	5580	4.50	0.644	14.388	15.863	0.00	1226.85
Kepler-295	0.90	-	5603	4.44	0.717	13.145	14.631	0.00	1699.19
Kepler-296	0.48	0.50	3740	4.77	0.040	13.391	16.363	-0.08	-1.00
Kepler-298	0.58	-	4465	4.71	0.120	13.718	15.617	0.00	518.20
Kepler-299	1.03	-	5617	4.39	0.949	13.875	15.232	0.00	1052.24
Kepler-303	0.48	-	3944	4.77	0.050	12.410	14.917	0.00	209.74
Kepler-316	0.52	-	4204	4.74	0.076	13.324	15.810	0.00	384.94
Kepler-32	0.53	0.58	3900	4.64	0.058	13.616	16.360	0.00	323.85
Kepler-327	0.49	-	3799	4.76	0.045	12.794	15.611	0.00	241.99
Kepler-329	0.52	-	4257	4.74	0.080	13.513	15.886	0.00	439.72
Kepler-330	0.72	-	5117	4.64	0.319	13.860	15.569	0.00	717.53
Kepler-331	0.49	-	4347	4.77	0.077	14.082	16.199	0.00	580.12
Kepler-332	0.72	-	4955	4.61	0.281	12.558	14.243	0.00	344.19
Kepler-333	0.53	-	4259	4.73	0.083	12.860	15.052	0.00	324.41
Kepler-341	1.02	-	6012	4.44	1.221	13.416	14.739	0.00	1047.03
Kepler-345	0.62	-	4504	4.68	0.142	12.309	14.344	0.00	-1.00
Kepler-353	0.50	-	3903	4.75	0.052	13.601	16.126	0.00	384.69
Kepler-354	0.67	-	4648	4.63	0.188	13.875	15.771	0.00	554.06
Kepler-362	0.72	-	5788	4.64	0.523	13.322	14.608	0.00	1090.51
Kepler-367	0.69	-	4710	4.63	0.210	11.243	13.193	0.00	188.03
Kepler-369	0.47	-	3591	4.79	0.033	13.247	16.429	0.00	-1.00
Kepler-37	0.77	0.80	5417	4.57	0.459	8.356	9.770	-0.32	63.92
Kepler-371	0.99	-	5666	4.39	0.907	12.701	13.997	0.00	813.19
Kepler-378	0.67	-	4661	4.65	0.190	10.846	12.619	0.00	152.09
Kepler-383	0.67	-	4710	4.62	0.198	13.367	15.473	0.00	-1.00
Kepler-384	0.88	-	5577	4.47	0.673	12.419	13.734	0.00	895.68
Kepler-386	0.77	-	5178	4.56	0.383	14.183	15.949	0.00	882.46
Kepler-388	0.59	-	4498	4.69	0.128	13.261	15.218	0.00	-1.00
Kepler-395	0.56	-	4262	4.73	0.093	13.818	16.592	0.00	421.38
Kepler-398	0.61	-	4493	4.69	0.136	11.514	13.499	0.00	177.36
Kepler-399	0.68	-	5502	4.62	0.381	13.175	14.686	0.00	740.54
Kepler-403	1.33	-	6090	4.27	2.186	11.830	12.818	0.00	840.27
Kepler-409	0.89	0.92	5460	4.50	0.632	8.200	9.636	0.08	68.17
Kepler-42	0.17	0.13	3068	-	0.002	12.177	16.700	-0.33	40.06
Kepler-430	1.49	1.17	5884	4.15	2.391	12.743	13.908	0.20	917.48
Kepler-438	0.52	0.54	3748	4.74	0.044	12.130	15.104	0.16	-1.00
Kepler-440	0.56	0.57	4134	4.71	0.079	12.960	15.637	-0.30	301.03
Kepler-445	0.21	0.18	3157	-	0.004	13.542	18.190	0.27	127.20
Kepler-446	0.24	0.22	3359	-	0.007	13.591	17.504	-0.30	96.34
Kepler-452	1.11	1.04	5757	4.32	1.216	12.263	13.540	0.21	551.73
Kepler-49	0.56	-	4252	4.73	0.092	13.184	15.655	0.00	311.22
Kepler-504	0.33	0.33	3519	4.94	0.015	12.000	15.143	-0.31	99.07
Kepler-52	0.52	0.54	4075	4.74	0.067	13.153	15.513	0.00	321.54
Kepler-54	0.50	0.51	3705	4.75	0.042	13.508	16.282	0.00	271.70
Kepler-55	0.62	-	4503	4.68	0.142	13.970	15.746	0.00	578.80
Kepler-560	0.33	0.34	3556	4.94	0.016	12.276	15.660	-0.39	109.31
Kepler-62	0.64	0.69	4925	4.68	0.210	12.256	13.965	-0.37	300.87

Table 2 *continued*

Table 2 (*continued*)

Host Star	R (R _⊕)	M (M _⊕)	Teff	logg	L (L _⊕)	Jmag	Vmag	[Fe/H] (dex)	Dist
Kepler-69	0.93	0.81	5638	4.40	0.800	12.631	13.866	-0.29	730.63
Kepler-737	0.48	0.51	3813	4.77	0.044	12.910	15.971	-0.24	205.12
Kepler-779	0.44	0.46	3804	4.81	0.036	13.441	16.303	-0.43	283.16
Kepler-795	0.96	0.94	5631	4.45	0.832	12.143	13.423	-0.02	492.12
Kepler-80	0.68	0.83	4540	4.64	0.176	12.954	15.230	0.04	369.45
Kepler-801	0.63	0.67	4435	4.66	0.138	13.489	15.596	-0.17	440.43
Kepler-81	0.59	-	4500	4.70	0.128	13.168	15.258	0.00	348.29
Kepler-85	0.89	-	5436	4.49	0.621	13.552	14.890	0.00	765.03
Kepler-878	0.77	0.81	5044	4.58	0.345	13.363	14.967	-0.03	791.63
Kepler-888	0.90	0.97	5875	4.52	0.867	11.915	13.061	-0.21	420.82
Kepler-916	0.81	0.85	5248	4.56	0.447	13.838	15.363	-0.05	830.71
Kepler-973	0.78	0.86	5213	4.58	0.404	11.845	13.478	-0.06	328.52
Kepler-974	0.50	0.52	3687	4.76	0.042	11.951	15.295	0.07	134.31
Kepler-992	0.74	0.80	4944	4.60	0.294	11.899	13.557	-0.04	259.64
L 98-59	0.30	0.27	3415	4.86	0.011	7.933	11.685	-0.46	10.62
LHS 1140	0.21	0.19	2988	-	0.003	9.612	14.150	-0.26	14.99
LHS 1478	0.25	0.24	3381	4.87	0.007	9.615	13.304	-0.13	18.23
LHS 1678	0.33	0.34	3490	-	0.014	9.020	12.600	0.00	19.88
LP 791-18	0.17	0.14	2960	5.12	0.002	11.559	16.910	-0.09	26.49
LP 890-9	0.16	0.12	2850	5.13	0.001	12.258	18.000	-0.03	32.43
TTT 1445 A	0.27	0.26	3340	-	0.008	7.294	10.590	-0.34	6.87
Proxima Cen	0.14	0.12	3050	-	0.002	5.357	11.010	0.00	1.30
Ross 128	0.20	0.17	3192	-	0.004	6.505	11.120	-0.02	3.37
Ross 508	0.21	0.18	3071	5.04	0.004	9.105	14.180	-0.20	11.21
TOI-1266	0.42	0.45	3600	4.85	0.027	9.706	12.941	-0.50	36.01
TOI-1452	0.28	0.25	3185	4.95	0.007	10.604	14.354	-0.07	30.52
TOI-2285	0.46	0.45	3491	-	0.029	9.860	13.403	-0.05	42.41
TOI-237	0.21	0.18	3212	5.04	0.004	11.740	16.370	0.00	38.07
TOI-270	0.38	0.39	3506	4.87	0.019	9.099	12.603	-0.20	22.48
TOI-540	0.19	0.16	3216	-	0.003	9.755	14.823	0.00	14.00
TOI-700	0.42	0.41	3461	4.80	0.023	9.469	13.151	-0.07	31.13
TOI-776	0.54	0.54	3709	4.73	0.049	8.483	11.536	-0.20	27.17
TRAPPIST-1	0.12	0.09	2566	5.24	0.001	11.354	17.020	0.00	-1.00
Teegarden's Star	0.11	0.09	2904	-	0.001	8.394	15.130	-0.19	3.83
Wolf 1061	0.31	0.29	3342	-	0.010	5.950	10.100	-0.09	4.31
YZ Cet	0.16	0.14	3151	5.17	0.002	-	-	-0.18	3.71

ACKNOWLEDGEMENTS

The authors acknowledge support from NASA grant 80NSSC21K1797, and KB acknowledges the support of NASA grant 80NSSC20K1529, both of which are funded through the NASA Habitable Worlds Program. T.F. acknowledges support from the University of California President's Postdoctoral Fellowship Program. This research has made use of the NASA Exoplanet Archive,

which is operated by the California Institute of Technology, under contract with the National Aeronautics and Space Administration under the Exoplanet Exploration Program. The results reported herein benefited from collaborations and/or information exchange within NASA's Nexus for Exoplanet System Science (NExSS) research coordination network sponsored by NASA's Science Mission Directorate.

Software: Matplotlib (Hunter 2007), NumPy (Harris et al. 2020), SciPy (Virtanen et al. 2020), pandas (Reback et al. 2020)

REFERENCES

- Agol, E., Dorn, C., Grimm, S. L., et al. 2021, The planetary science journal, 2, 1
- Akeson, R. L., Chen, X., Ciardi, D., et al. 2013, PASP, 125, 989, doi: [10.1088/0031-429X/125/916/989](https://doi.org/10.1088/0031-429X/125/916/989)

- Anglada-Escudé, G., Amado, P. J., Barnes, J., et al. 2016, *Nature*, 536, 437
- Astudillo-Defru, N., Forveille, T., Bonfils, X., et al. 2017, *Astronomy & Astrophysics*, 602, A88
- Bagnasco, G., Kolm, M., Ferruit, P., et al. 2007, in *Cryogenic Optical Systems and Instruments XII*, Vol. 6692, SPIE, 174–187
- Barstow, J. K., Aigrain, S., Irwin, P. G., Kendrew, S., & Fletcher, L. N. 2016, *Monthly Notices of the Royal Astronomical Society*, 458, 2657
- Batalha, N. E., Lewis, N. K., Line, M. R., Valenti, J., & Stevenson, K. 2018, *ApJL*, 856, L34, doi: [10.3847/2041-8213/aab896](https://doi.org/10.3847/2041-8213/aab896)
- Bixel, A., & Apai, D. 2017, *ApJL*, 836, L31, doi: [10.3847/2041-8213/aa5f51](https://doi.org/10.3847/2041-8213/aa5f51)
- Bonfils, X., Almenara, J.-M., Cloutier, R., et al. 2018, *Astronomy & Astrophysics*, 618, A142
- Borucki, W. J., Koch, D., Basri, G., et al. 2010, *Science*, 327, 977, doi: [10.1126/science.1185402](https://doi.org/10.1126/science.1185402)
- Butler, R. P., Wright, J. T., Marcy, G. W., et al. 2006, *ApJ*, 646, 505, doi: [10.1086/504701](https://doi.org/10.1086/504701)
- Butler, R. P., Vogt, S. S., Laughlin, G., et al. 2017, *AJ*, 153, 208, doi: [10.3847/1538-3881/aa66ca](https://doi.org/10.3847/1538-3881/aa66ca)
- Byrne, P. K., Ghail, R. C., Gilmore, M. S., et al. 2021, *Geology*, 49, 81
- Cascioli, G., Hensley, S., De Marchi, F., et al. 2021, *The Planetary Science Journal*, 2, 220
- Chandler, C. O., McDonald, I., & Kane, S. R. 2016, *AJ*, 151, 59, doi: [10.3847/0004-6256/151/3/59](https://doi.org/10.3847/0004-6256/151/3/59)
- Chen, J., & Kipping, D. 2017, *ApJ*, 834, 17, doi: [10.3847/1538-4357/834/1/17](https://doi.org/10.3847/1538-4357/834/1/17)
- Demangeon, O. D., Osorio, M. Z., Alibert, Y., et al. 2021, *Astronomy & Astrophysics*, 653, A41
- Demory, B.-O., Pozuelos, F., Chew, Y. G. M., et al. 2020, *Astronomy & Astrophysics*, 642, A49
- Donahue, T. M., Hoffman, J. H., Hodges, R. R., & Watson, A. J. 1982, *Science*, 216, 630, doi: [10.1126/science.216.4546.630](https://doi.org/10.1126/science.216.4546.630)
- Doyon, R., Hutchings, J. B., Beaulieu, M., et al. 2012, in *Space Telescopes and Instrumentation 2012: Optical, Infrared, and Millimeter Wave*, Vol. 8442, SPIE, 1005–1017
- Dreizler, S., Jeffers, S., Rodríguez, E., et al. 2020, *Monthly Notices of the Royal Astronomical Society*, 493, 536
- Ehrenreich, D., Vidal-Madjar, A., Widemann, T., et al. 2012, *A&A*, 537, L2, doi: [10.1051/0004-6361/201118400](https://doi.org/10.1051/0004-6361/201118400)
- Fauchez, T. J., Turbet, M., Sergeev, D. E., et al. 2021, *PSJ*, 2, 106, doi: [10.3847/PSJ/abf4df](https://doi.org/10.3847/PSJ/abf4df)
- Fischer, D. A., Marcy, G. W., & Spronck, J. F. P. 2014, *ApJS*, 210, 5, doi: [10.1088/0067-0049/210/1/5](https://doi.org/10.1088/0067-0049/210/1/5)
- Fischer, D. A., Anglada-Escude, G., Arriagada, P., et al. 2016, *PASP*, 128, 066001, doi: [10.1088/1538-3873/128/964/066001](https://doi.org/10.1088/1538-3873/128/964/066001)
- Foley, B. J. 2019, *The Astrophysical Journal*, 875, 72
- Foley, B. J., & Smye, A. J. 2018, *Astrobiology*, 18, 873
- Ford, E. B. 2014, *Proceedings of the National Academy of Sciences*, 111, 12616, doi: [10.1073/pnas.1304219111](https://doi.org/10.1073/pnas.1304219111)
- Fujii, Y., Angerhausen, D., Deitrick, R., et al. 2018, *Astrobiology*, 18, 739, doi: [10.1089/ast.2017.1733](https://doi.org/10.1089/ast.2017.1733)
- Fukui, A., Kimura, T., Hirano, T., et al. 2022, *Publications of the Astronomical Society of Japan*, 74, L1
- Fulton, B. J., Petigura, E. A., Howard, A. W., et al. 2017, *AJ*, 154, 109, doi: [10.3847/1538-3881/aa80eb](https://doi.org/10.3847/1538-3881/aa80eb)
- Fulton, B. J., Rosenthal, L. J., Hirsch, L. A., et al. 2021, *ApJS*, 255, 14, doi: [10.3847/1538-4365/abfcc1](https://doi.org/10.3847/1538-4365/abfcc1)
- Gaia Collaboration, Brown, A. G. A., Vallenari, A., et al. 2016, *A&A*, 595, A2, doi: [10.1051/0004-6361/201629512](https://doi.org/10.1051/0004-6361/201629512)
- Gaia Collaboration, Vallenari, A., Brown, A. G. A., et al. 2022, arXiv e-prints, arXiv:2208.00211, <https://arxiv.org/abs/2208.00211>
- Gao, P., Hu, R., Robinson, T. D., Li, C., & Yung, Y. L. 2015, *The Astrophysical Journal*, 806, 249, doi: [10.1088/0004-637X/806/2/249](https://doi.org/10.1088/0004-637X/806/2/249)
- Garvin, J. B., Getty, S. A., Arney, G. N., et al. 2022, *The Planetary Science Journal*, 3, 117
- Gaudi, B. S., Seager, S., Mennesson, B., et al. 2020, arXiv e-prints, arXiv:2001.06683, <https://arxiv.org/abs/2001.06683>
- Gupta, A. F., Wright, J. T., Robertson, P., et al. 2021, *AJ*, 161, 130, doi: [10.3847/1538-3881/abd79e](https://doi.org/10.3847/1538-3881/abd79e)
- Hamano, K., Abe, Y., & Genda, H. 2013, *Nature*, 497, 607, doi: [10.1038/nature12163](https://doi.org/10.1038/nature12163)
- Harris, C. R., Millman, K. J., Van Der Walt, S. J., et al. 2020, *Nature*, 585, 357
- Head, J. W. 2014, *Geology*, 42, 95
- Head, J. W., & Solomon, S. C. 1981, *Science*, 213, 62
- Head, J. W., Wilson, L., Ivanov, M. A., & Wordsworth, R. 2021, in *LPI Contributions*, Vol. 2628, LPI Contributions, 8023
- Head, J. W., Wood, C. A., & Mutch, T. A. 1977, *American Scientist*, 65, 21
- Head, J. W., Yuter, S. E., & Solomon, S. C. 1981, *American Scientist*, 69, 614
- Head III, J. W., & Crumpler, L. 1987, *Science*, 238, 1380
- Hill, M. L., Bott, K., Dalba, P. A., et al. 2023, *The Astronomical Journal*, 165, 34
- Horner, J., Kane, S. R., Marshall, J. P., et al. 2020, *PASP*, 132, 102001, doi: [10.1088/1538-3873/ab8eb9](https://doi.org/10.1088/1538-3873/ab8eb9)
- Hu, R., Peterson, L., & Wolf, E. T. 2020, *The Astrophysical Journal*, 888, 122

- Hunter, J. D. 2007, Computing in science & engineering, 9, 90
- Ivanov, P. B., & Papaloizou, J. C. B. 2011, Celestial Mechanics and Dynamical Astronomy, 111, 51, doi: [10.1007/s10569-011-9367-x](https://doi.org/10.1007/s10569-011-9367-x)
- Kaltenegger, L., Pepper, J., Stassun, K., & Oelkers, R. 2019, ApJL, 874, L8, doi: [10.3847/2041-8213/ab0e8d](https://doi.org/10.3847/2041-8213/ab0e8d)
- Kane, S. R., Gelino, D. M., & Turnbull, M. C. 2017, AJ, 153, 52, doi: [10.3847/1538-3881/153/2/52](https://doi.org/10.3847/1538-3881/153/2/52)
- Kane, S. R., Kopparapu, R. K., & Domagal-Goldman, S. D. 2014, ApJL, 794, L5, doi: [10.1088/2041-8205/794/1/L5](https://doi.org/10.1088/2041-8205/794/1/L5)
- Kane, S. R., Hill, M. L., Kasting, J. F., et al. 2016, ApJ, 830, 1, doi: [10.3847/0004-637X/830/1/1](https://doi.org/10.3847/0004-637X/830/1/1)
- Kane, S. R., Arney, G., Crisp, D., et al. 2019, Journal of Geophysical Research (Planets), 124, 2015, doi: [10.1029/2019JE005939](https://doi.org/10.1029/2019JE005939)
- Kane, S. R., Arney, G. N., Byrne, P. K., et al. 2021, Journal of Geophysical Research (Planets), 126, e06643, doi: [10.1002/jgre.v126.2](https://doi.org/10.1002/jgre.v126.2)
- Kasting, J. F. 1988, Icarus, 74, 472, doi: [10.1016/0019-1035\(88\)90116-9](https://doi.org/10.1016/0019-1035(88)90116-9)
- Kasting, J. F., Whitmire, D. P., & Reynolds, R. T. 1993, Icarus, 101, 108, doi: [10.1006/icar.1993.1010](https://doi.org/10.1006/icar.1993.1010)
- Kempton, E. M. R., Bean, J. L., Louie, D. R., et al. 2018, PASP, 130, 114401, doi: [10.1088/1538-3873/aadf6f](https://doi.org/10.1088/1538-3873/aadf6f)
- Khawja, S., Ernst, R., Samson, C., et al. 2020, Nature communications, 11, 1
- Kopparapu, R. K., Ramirez, R. M., SchottelKotte, J., et al. 2014, ApJ, 787, L29, doi: [10.1088/2041-8205/787/2/L29](https://doi.org/10.1088/2041-8205/787/2/L29)
- Kopparapu, R. K., Ramirez, R., Kasting, J. F., et al. 2013, ApJ, 765, 131, doi: [10.1088/0004-637X/765/2/131](https://doi.org/10.1088/0004-637X/765/2/131)
- Li, Z., Hildebrandt, S. R., Kane, S. R., et al. 2021, AJ, 162, 9, doi: [10.3847/1538-3881/abf831](https://doi.org/10.3847/1538-3881/abf831)
- Lillo-Box, J., Figueira, P., Leleu, A., et al. 2020, Astronomy & Astrophysics, 642, A121
- Limbach, M. A., & Turner, E. L. 2015, Proceedings of the National Academy of Science, 112, 20, doi: [10.1073/pnas.1406545111](https://doi.org/10.1073/pnas.1406545111)
- Lincowski, A. P., Lustig-Yaeger, J., & Meadows, V. S. 2019, AJ, 158, 26, doi: [10.3847/1538-3881/ab2385](https://doi.org/10.3847/1538-3881/ab2385)
- Lincowski, A. P., Meadows, V. S., Crisp, D., et al. 2018, The Astrophysical Journal, 867, 76, doi: [10.3847/1538-4357/aae36a](https://doi.org/10.3847/1538-4357/aae36a)
- Lopez, E. D., & Fortney, J. J. 2013, The Astrophysical Journal, 776, 2
- Lovis, C., Fischer, D., et al. 2010, Exoplanets, 27
- Luger, R., & Barnes, R. 2015, Astrobiology, 15, 119, doi: [10.1089/ast.2014.1231](https://doi.org/10.1089/ast.2014.1231)
- Luque, R., Pallé, E., Kossakowski, D., et al. 2019, Astronomy & Astrophysics, 628, A39
- Luque, R., Serrano, L., Molaverdikhani, K., et al. 2021, Astronomy & Astrophysics, 645, A41
- Lustig-Yaeger, J., Meadows, V. S., & Lincowski, A. P. 2019, AJ, 158, 27, doi: [10.3847/1538-3881/ab21e0](https://doi.org/10.3847/1538-3881/ab21e0)
- Mandell, A. M., Lustig-Yaeger, J., Stevenson, K., & Staguhn, J. 2022, MIRECLE: Science Yield for a Mid-IR Explorer-Class Mission to Study Non-Transiting Rocky Planets Orbiting the Nearest M-Stars Using Planetary Infrared Excess, arXiv, doi: [10.48550/ARXIV.2207.13727](https://doi.org/10.48550/ARXIV.2207.13727)
- Martin, R. G., & Livio, M. 2015, ApJ, 810, 105, doi: [10.1088/0004-637X/810/2/105](https://doi.org/10.1088/0004-637X/810/2/105)
- McKinnon, W. B., Zahnle, K. J., Ivanov, B. A., & Melosh, H. 1997, Venus II: Geology, geophysics, atmosphere, and solar wind environment, 969
- Meadows, V. S., Reinhard, C. T., Arney, G. N., et al. 2018, Astrobiology, 18, 630, doi: [10.1089/ast.2017.1727](https://doi.org/10.1089/ast.2017.1727)
- Morley, C. V., Kreidberg, L., Rustamkulov, Z., Robinson, T., & Fortney, J. J. 2017, ApJ, 850, 121, doi: [10.3847/1538-4357/aa927b](https://doi.org/10.3847/1538-4357/aa927b)
- NASA Exoplanet Archive. 2023, Planetary Systems, Version: 2023-01-19, NExScI-Caltech/IPAC, doi: [10.26133/NEA12](https://doi.org/10.26133/NEA12)
- Ostberg, C., & Kane, S. R. 2019, AJ, 158, 195, doi: [10.3847/1538-3881/ab44b0](https://doi.org/10.3847/1538-3881/ab44b0)
- Owen, J. E., & Wu, Y. 2013, The Astrophysical Journal, 775, 105
- Pepe, F., Molero, P., Cristiani, S., et al. 2014, Astronomische Nachrichten, 335, 8, doi: [10.1002/asna.201312004](https://doi.org/10.1002/asna.201312004)
- Pidhorodetska, D., Moran, S. E., Schwieterman, E. W., et al. 2021, The Astronomical Journal, 162, 169
- Reback, J., McKinney, W., Van Den Bossche, J., et al. 2020, Zenodo
- Ricker, G. R., Winn, J. N., Vanderspek, R., et al. 2015, Journal of Astronomical Telescopes, Instruments, and Systems, 1, 014003, doi: [10.1117/1.JATIS.1.1.014003](https://doi.org/10.1117/1.JATIS.1.1.014003)
- Roberge, A., Rizzo, M. J., Lincowski, A. P., et al. 2017, PASP, 129, 124401, doi: [10.1088/1538-3873/aa8fc4](https://doi.org/10.1088/1538-3873/aa8fc4)
- Rogers, L. A. 2015, ApJ, 801, 41, doi: [10.1088/0004-637X/801/1/41](https://doi.org/10.1088/0004-637X/801/1/41)
- Rosenthal, L. J., Fulton, B. J., Hirsch, L. A., et al. 2021, ApJS, 255, 8, doi: [10.3847/1538-4365/abe23c](https://doi.org/10.3847/1538-4365/abe23c)
- Schaefer, L., Wordsworth, R. D., Berta-Thompson, Z., & Sasselov, D. 2016, The Astrophysical Journal, 829, 63, doi: [10.3847/0004-637X/829/2/63](https://doi.org/10.3847/0004-637X/829/2/63)
- Schwieterman, E. W., Meadows, V. S., Domagal-Goldman, S. D., et al. 2016, The Astrophysical Journal, 819, L13, doi: [10.3847/2041-8205/819/1/L13](https://doi.org/10.3847/2041-8205/819/1/L13)
- Schwieterman, E. W., Kiang, N. Y., Parenteau, M. N., et al. 2018, Astrobiology, 18, 663, doi: [10.1089/ast.2017.1729](https://doi.org/10.1089/ast.2017.1729)

- Solomon, S. C., Head, J. W., Kaula, W. M., et al. 1991, *Science*, 252, 297
- Solomon, S. C., Smrekar, S. E., Bindschadler, D. L., et al. 1992, *Journal of Geophysical Research: Planets*, 97, 13199
- Stefansson, G., Hearty, F., Robertson, P., et al. 2016, *ApJ*, 833, 175, doi: [10.3847/1538-4357/833/2/175](https://doi.org/10.3847/1538-4357/833/2/175)
- The LUVOIR Team. 2019, arXiv preprint 1912.06219. <https://arxiv.org/abs/1912.06219>
- Tian, F. 2015, *Earth and Planetary Science Letters*, 432, 126, doi: [10.1016/j.epsl.2015.09.051](https://doi.org/10.1016/j.epsl.2015.09.051)
- Tremaine, S., & Dong, S. 2012, *AJ*, 143, 94, doi: [10.1088/0004-6256/143/4/94](https://doi.org/10.1088/0004-6256/143/4/94)
- Trifonov, T., Tal-Or, L., Zechmeister, M., et al. 2020, *A&A*, 636, A74, doi: [10.1051/0004-6361/201936686](https://doi.org/10.1051/0004-6361/201936686)
- Turbet, M., Bolmont, E., Chaverot, G., et al. 2021, *Nature*, 598, 276, doi: [10.1038/s41586-021-03873-w](https://doi.org/10.1038/s41586-021-03873-w)
- Turbet, M., Bolmont, E., Chaverot, G., et al. 2021, *Nature*, 598, 276
- Udry, S., & Santos, N. C. 2007, *ARA&A*, 45, 397, doi: [10.1146/annurev.astro.45.051806.110529](https://doi.org/10.1146/annurev.astro.45.051806.110529)
- Unterborn, C. T., Dismukes, E. E., & Panero, W. R. 2016, *ApJ*, 819, 32, doi: [10.3847/0004-637X/819/1/32](https://doi.org/10.3847/0004-637X/819/1/32)
- Unterborn, C. T., Foley, B. J., Desch, S. J., et al. 2022, *The Astrophysical Journal Letters*, 930, L6
- Unterborn, C. T., & Panero, W. R. 2019, *Journal of Geophysical Research (Planets)*, 124, 1704, doi: [10.1029/2018JE005844](https://doi.org/10.1029/2018JE005844)
- Van Eylen, V., Agentoft, C., Lundkvist, M., et al. 2018, *Monthly Notices of the Royal Astronomical Society*, 479, 4786
- Virtanen, P., Gommers, R., Oliphant, T. E., et al. 2020, *Nature methods*, 17, 261
- Vorontsov, V., Lokhmatova, M., Martynov, M., et al. 2011, *Solar System Research*, 45, 710
- Way, M. J., & Del Genio, A. D. 2020, *Journal of Geophysical Research (Planets)*, 125, e06276, doi: [10.1029/2019JE006276](https://doi.org/10.1029/2019JE006276)
- Way, M. J., Del Genio, A. D., Kiang, N. Y., et al. 2016, *Geophys. Res. Lett.*, 43, 8376, doi: [10.1002/2016GL069790](https://doi.org/10.1002/2016GL069790)
- Way, M. J., Aleinov, I., Amundsen, D. S., et al. 2017, *ApJS*, 231, 12, doi: [10.3847/1538-4365/aa7a06](https://doi.org/10.3847/1538-4365/aa7a06)
- Widemann, T., Ghail, R., Wilson, C. F., & Titov, D. V. 2020, in *Agu fall meeting abstracts*, Vol. 2020, P022–02
- Winn, J. N., & Fabrycky, D. C. 2015, *ARA&A*, 53, 409, doi: [10.1146/annurev-astro-082214-122246](https://doi.org/10.1146/annurev-astro-082214-122246)
- Winters, J. G., Cloutier, R., Medina, A. A., et al. 2022, *The Astronomical Journal*, 163, 168
- Wolf, E. T., Kopparapu, R., Haqq-Misra, J., & Fauchez, T. J. 2022, *PSJ*, 3, 7, doi: [10.3847/PSJ/ac3f3d](https://doi.org/10.3847/PSJ/ac3f3d)
- Wright, G. S., Rieke, G. H., Colina, L., et al. 2004, in *Optical, Infrared, and Millimeter Space Telescopes*, Vol. 5487, SPIE, 653–663
- Zahnle, K. J., & Catling, D. C. 2017, *ApJ*, 843, 122, doi: [10.3847/1538-4357/aa7846](https://doi.org/10.3847/1538-4357/aa7846)
- Zasova, L., Gorinov, D., Eismont, N., et al. 2019, *Solar System Research*, 53, 506
- Zechmeister, M., Dreizler, S., Ribas, I., et al. 2019, *Astronomy & Astrophysics*, 627, A49